

Pleiades Binary Fraction Revisited

DMITRY CHULKOV ¹

¹*Institute of Astronomy of the Russian Academy of Sciences (INASAN) 119017, Pyatnitskaya st., 48, Moscow, Russia*

ABSTRACT

One of the nearest and best studied open clusters, Pleiades is an important cornerstone of stellar astrophysics. Despite its role as reference coeval stellar population, its multiplicity properties remain vaguely determined. The combined use of Gaia DR3 multiband photometry, astrometric parameter RUWE, non-single star solutions along with available ground-based spectroscopic, high angular resolution, and polarimetric observations enable more robust constraints on the binary star population in the cluster. Several conclusions may have broader implications for other stellar populations. Twin binaries, with mass ratio close to $q \sim 1$, tend to have lower RUWE, increasing their membership selection probability, relative to $q \sim 0.5$ systems that are disfavored. The frequently observed peak in mass ratio distribution for $q \sim 1$ binaries may be partially attributed to this bias. Photometrically fitted mass ratio is underestimated for double-lined spectroscopic binaries in agreement with other authors. Differential extinction photometrically mimics stellar binarity. An area of enlarged absorption is traced by increased polarization south of the Merope star and excluded from the analysis to avoid this bias. The fraction of systems with $q > 0.6$ companions is measured to be $f = 16.4\%_{-0.6}^{+2.6}$ for $m > 0.5 M_{\odot}$ stars, which is larger than recent Gaia-based estimates, but compatible with the pre-Gaia values for Pleiades and the field population. Binary fraction shows no steady increase with stellar mass in the $0.5 - 1.2 M_{\odot}$ range, while mass ratio has a bimodal distribution with a minimum near $q \sim 0.7$.

1. INTRODUCTION

Pleiades has been an important reference object for astronomers for centuries. Indeed, the description of the Pleiades appears in the influential work by Galileo Galilei, who described his first telescopic observations back in 1610 (A. Longhin 2025). Stellar multiplicity is an inherent property of any stellar population (G. Duchêne & A. Kraus 2013). Pleiades stars are frequently used as a testing ground for different aspects of stellar astrophysics and a detailed review of their multiplicity is desirable for credible data interpretation. Despite dedicated efforts through the years, the constraints on Pleiades multiplicity remain significantly incomplete.

Gaia space observatory (Gaia Collaboration et al. 2016) has advanced our knowledge of the cosmos on different scales from the Solar System to the distant galaxies (M. Perryman 2025) and brought a tremendous breakthrough for the census of Galactic open clusters (T. Cantat-Gaudin & L. Casamiquela 2024) and binary stars in the stellar neighborhood (K. El-Badry 2024). The reported multiplicity fraction in open clusters varies in a surprisingly wide range (G. Cordoni et al. 2023; J.

Donada et al. 2023), which raises the possibility of unaccounted biases. Observations coming from diverse data sets allow for more robust constraints on stellar multiplicity (C. Cifuentes et al. 2025), and this paper aims to reevaluate the binary star population in the Pleiades.

In Section 2 the sample of Pleiades stars is defined. Several multiplicity indicators are considered, starting from spectroscopic binarity in Section 3, followed by parameter RUWE in Section 4. Gaia non-single star solutions are explored in Section 5. In Section 6 binary parameters are retrieved from color-magnitude diagram analysis, which is the principal method in this study. Differential extinction that may photometrically resemble binarity is discussed in Sections 6.4 – 6.6. Finally, the binary fraction is constrained in Section 7, and the key conclusions are briefly summarized in Section 8.

2. CLUSTER MEMBERS

Cluster member selection usually relies on analysis of astrometric, photometric and spectroscopic data, preferably in their combination. All these data channels are compromised in case of binary or multiple stars, thus obstructing correct membership classification. It became possible to trace Pleiades tidal arms for at least 200 pc or 70 degrees in the celestial sphere (D. Risbud et al. 2025) and possibly even further (J. Kos 2024). How-

ever, these studies are largely based on the single-star solutions which make up the main source Gaia DR3 catalog (Gaia Collaboration et al. 2021). Relating a binary star with poorly-fitted astrometric solution to its parent cluster, especially at a large distance from the center is challenging, and to mitigate the arising biases auxiliary data sets should be considered in addition to Gaia.

Table 2 from D. Chulkov (2024) is adopted as an initial list of probable Pleiades members. It includes Gaia DR3 entries with $G < 15$ mag within 2° of the cluster’s center. Of these, 409 were deemed probable members, and membership was questioned for another 14. The often ignored sources with unreliable Gaia DR3 astrometric solutions are included thanks to ground-based proper motion data from the PPMXL catalog (S. Roeser et al. 2010) and radial velocities from several datasets. Spectroscopic data become scarce at $G \gtrsim 15$ mag, thus obstructing the extension toward fainter objects. For all considered sources, homogeneous high angular resolution observations were carried out (D. Chulkov et al. 2025), enabling the identification of binary stars in the subarcsecond angular separation range ($0.1 \lesssim \rho \lesssim 1''$).

The available data continue to grow, and the Sloan Digital Sky Survey (SDSS) data release 19 (SDSS Collaboration et al. 2025) has brought new radial velocity estimates (S. Mészáros et al. 2025) based on a reanalysis of previously obtained spectra. This allows reconsidering the status of LV Tau ($G = 14.89$ mag) whose astrometric solution and photometric data are consistent with cluster membership, but the reported radial velocities in Gaia DR3 and SDSS DR17 catalogs fall far from the cluster’s average of 5.69 ± 0.07 km s $^{-1}$ (G. Torres et al. 2021). The new value, 1.5 ± 2.2 km s $^{-1}$, enables the reclassification of LV Tau as a probable Pleiades member, bringing the total number of considered sources to 410. The complete list of entries is provided in Table 4.

3. SPECTROSCOPIC BINARIES

The observation of periodic variations in the position of spectral lines due to Doppler shift is one of the fundamental methods to detect binarity (H. Sana & J. Vrancken 2025). The discovery and parametrization of spectroscopic binaries depend on many factors which impose a heavy bias for the obtained subsample (G. Torres et al. 2021), and many genuine systems are hardly detectable spectroscopically, such as ones with low inclination (face-on) orbits. Thus, rapid rotation typical for Pleiades stars causes line broadening which complicates the radial velocity measurements (G. Torres 2020).

In a favorable case, the radial velocities of both components are measured from the observed spectra. The review of known double-lined (SB2) systems restricted

to our sample is given in Table 1. The mass ratio of components $q = m_2/m_1, m_2 \leq m_1$ may be estimated for a system with an orbital solution (J. Southworth 2020), which is available for 18 of the sample systems. Two sources, HD 23608 and HII 2027, show flux contribution from a third star, making them SB3 systems; their outer companions are resolved (D. Chulkov et al. 2025).

Generally, binarity can be detected in a single epoch spectroscopic observation (K. El-Badry et al. 2018). Ten sample sources were revealed as possible SB2 based on APOGEE data (M. Kounkel et al. 2021), with two of them, V759 Tau and LM Tau, currently without orbital solution in the literature. Analysis of LAMOST medium-resolution data from S.-s. Li et al. (2025) brought four SB2 candidates, including already known V888 Tau and V889 Tau. For V1065 Tau and V1271 Tau, the mass ratio is estimated based on radial velocities of components v_1 and v_2 , cluster mean and dispersion from G. Torres et al. (2021), $s = 5.69 \pm 0.48$ km s $^{-1}$, with a method from O. C. Wilson (1941):

$$q = \frac{v_1 - s}{s - v_2} \quad (1)$$

Y. Jing et al. (2025) after analysis of low resolution LAMOST spectra claimed binarity for 69 out of 410 sample objects based on training set with systems of mass ratios within $0.71 < q < 0.93$ range, 45 of them have low RUWE and no known resolved companions within $4''$ making them a convenient target for photometric confirmation (Section 6). However, only 16 sources show photometrically fitted $q > 0.4$ meaning that the majority of sources are indistinguishable from single stars, and this list is likely dominated by the false positive contamination and is not considered further.

From an orbital solution of SB2 systems the $m_1 \sin^3 i$ value can be derived, while inclination (i) and component masses ($m_{1,2}$) remain unknown (J. Southworth 2020). The availability of photometrically fitted masses (m_{ph}) derived in Section 6 allows a crude, model-dependent estimation of $\sin i$, which is given in Table 1:

$$\sin i = \sqrt[3]{\frac{m_1 \sin^3 i}{m_{\text{ph}}}} \quad (2)$$

For single-lined systems (SB1), only the value of $m_2 \sin i$ is derived, and q is not known from the orbital solution. Considering tables 6 and 12 from G. Torres et al. (2021), there are 21 SB1 binaries in the sample. While SB2 systems have a strong preference for large mass ratio, as lines from both components should be recovered in the spectra, SB1 binaries can have much lower secondary masses. Indeed, for 11 out of 21 entries the inferred value falls into $0.05 M_\odot \lesssim m_2 \sin i \lesssim 0.2 M_\odot$

Source	Name	G	RUWE	P	$m_1 \sin^3 i$	Mass ratio	Ref	Mass ratio	$\sin i$	
Gaia DR3		mag		days	M_\odot	q_{sp}		q_{ph}	q_{ph}^{L}	
66526127137440128	Atlas, 27 Tau	3.62	4.117	291	5.04 ± 0.17	0.72 ± 0.01	T25	$0.63^{+0.08}_{-0.07}$	0.55	0.95
66507469798631808	HD 23964A	6.81	0.974	16.7	1.53	0.55	T21	0.40	–	0.85
66729880383767168	V1229 Tau	6.82	1.145	2.46	2.14 ± 0.01	0.70	T21	0.54	0.47	0.95
66715174415764736	HD 23608	8.62	2-pam	7.76	0.75 ± 0.01	0.93	T21	SB3	–	–
69819404977607168	HD 23351	8.90	2.074	20.8	1.31 ± 0.03	0.62 ± 0.01	T21	$0.55^{+0.03}_{-0.03}$	0.53	0.97 ± 0.01
65090680344356992	HD 23158	9.43	6.012	269	1.30 ± 0.18	0.32 ± 0.02	T21	$0.34^{+0.08}_{-0.12}$	0.34	$1.00_{-0.03}$
65207709613871744	HD 23631B	9.74	3.377	767	0.91 ± 0.06	0.93 ± 0.02	T21	$0.72^{+0.03}_{-0.02}$	0.92	0.91 ± 0.02
65199978672758272	HD 282975	10.05	1.112	26.0	0.014	0.98 ± 0.01	T21	$0.75^{+0.00}_{-0.01}$	0.67	0.24
				26.0	0.059	0.95	S24			0.18
65276703968959488	HII 761	10.39	1.229	3.31	0.42 ± 0.01	0.68 ± 0.01	T21	$0.60^{+0.04}_{-0.02}$	0.54	0.73 ± 0.01
69883417170175488	HII 173	10.63	3.223	481	0.89 ± 0.02	0.95 ± 0.01	T21	$0.84^{+0.06}_{-0.03}$	0.74	0.97 ± 0.01
66720946851771904	HII 2027	10.71	2.419	48.6			T21	SB3	1	–
68310359628169088	V1084 Tau	10.85	5.585	757	0.68 ± 0.04	0.86 ± 0.02	T21	$0.89^{+0.10}_{-0.04}$	1.00	0.91 ± 0.02
64928605459180416	HII 2406	10.94	1.96	33.0	0.55 ± 0.04	0.54 ± 0.02	T21	< 0.3	0.26	0.83 ± 0.02
69876712724339456	V1271 Tau	11.43	1.114	–	–	0.69 ± 0.09	L25	$0.41^{+0.05}_{-0.00}$	0.56	–
64980278208557696	V1065 Tau	11.96	1.228	–	–	0.51 ± 0.03	L25	$0.84^{+0.06}_{-0.03}$	–	–
66734720809017856	HII 1348	12.23	1.652	94.8	0.31 ± 0.01	0.78 ± 0.01	T21	$0.78^{+0.03}_{-0.01}$	0.78	0.75 ± 0.01
65800930496992512	V888 Tau	12.52	1.091	3.11	0.59	0.99	T21	$0.96^{+0.00}_{-0.01}$	0.90	0.96
66612473157921024	V889 Tau	12.60	1.053	8.58	0.54 ± 0.01	0.98 ± 0.01	T21	$0.89^{+0.01}_{-0.00}$	0.80	0.92 ± 0.01
66937859881182848	V366 Tau	12.78	2.889	542	0.48 ± 0.04	0.82 ± 0.04	T21	$0.86^{+0.08}_{-0.02}$	1.00	0.90 ± 0.03
65005262035285888	QQ Tau	14.26	1.12	2.46	0.10	0.96 ± 0.02	F25	> 1	–	< 0.59
66722355601033600	V759 Tau	14.70	1.642	–	–	0.95 ± 0.08	K21	$0.77^{+0.06}_{-0.04}$	0.68	–
68259438496008832	LM Tau	14.77	1.579	–	–	–	K21	$0.52^{+0.05}_{-0.02}$	0.46	–

Table 1. Double-lined spectroscopic binaries among Pleiades sample stars. The reported period (P) uncertainties are less than 1% for all entries. q_{ph} is a photometrically fitted mass ratio (Section 6), q_{ph}^{L} is a best-fit estimate from R. Liu et al. (2025). Values of $q_{\text{ph}} < 0.5$ are generally unreliable; q_{ph} is not estimated for spectroscopic triple systems (SB3). References for spectroscopic solutions: F25 – A. Frasca et al. (2025), K21 – M. Kounkel et al. (2021), L25 – S.-s. Li et al. (2025), S24 – L. Sairam et al. (2024), T21 – G. Torres et al. (2021), T25 – G. Torres et al. (2025). For HD 282975 two options are shown. Mass ratios from K21 and L25 are not based on a complete orbital solution and, hence, less reliable; they are omitted from the comparison with q_{ph} in Section 6.3 and Figure 8. For V1065 Tau and QQ Tau, q_{ph} is probably overestimated due to enlarged extinction (Section 6.5). The $\sin i$ column is calculated from Equation 2; $i = 108^\circ$ is adopted for Atlas (G. Torres et al. 2025).

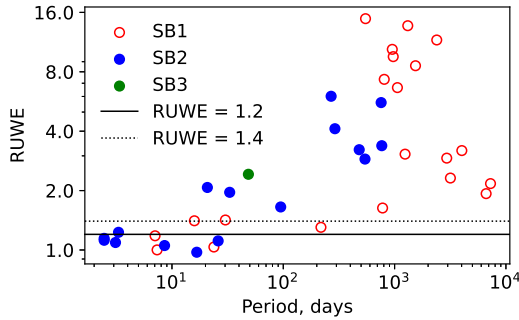


Figure 1. Reported orbital periods and RUWE values for spectroscopic systems. RUWE < 1.2 cutoff is used in Section 6.1 to select sources with reliable astrometric solutions.

range, making their photometric confirmation very hard. However, a large q remains possible, as for V1282 Tau (G. Torres et al. 2020), where the primary star has a

rapid rotation. SB1 systems tend to have larger periods (Figure 1) because smaller orbital velocities reduce the chance to detect lines from both components separately.

4. RUWE

4.1. Binarity indicator

Parameter RUWE (renormalized unit weight error) is a goodness-of-fit statistic used in Gaia catalogs that is a well-known indicator of stellar multiplicity (K. G. Stassun & G. Torres 2021). Its interpretation is not straightforward, as it involves at least two different modes for resolved and unresolved sources (V. Belokurov et al. 2020).

Gaia is an optical telescope with image sampling resolution of 0.059×0.177 arcsec per pixel depending on scan direction (B. Holl et al. 2023). For marginally resolved systems the point spread function is disturbed by the companion causing a photocenter displacement, and RUWE excess is consistently observed for pairs with an-

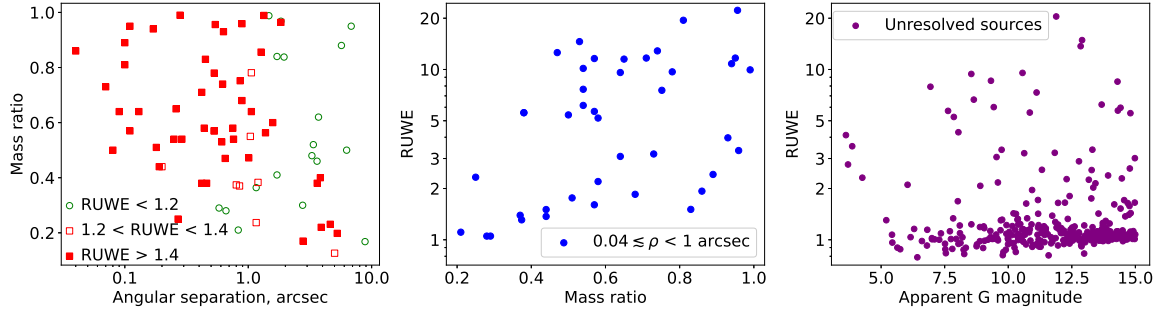


Figure 2. Left: RUWE for resolved sources depending on separation and mass ratio. When both components appear in Gaia DR3, RUWE of the brighter star is shown. Middle: RUWE for resolved sources with $\rho < 1''$; observational data are from D. Chulkov et al. (2025). Right: RUWE for sources without any resolved companions within $4''$ depending on G magnitude.

gular separation within one arcsec unless the secondary flux is too low (Figure 2). The vast majority of binaries with this mode of RUWE excess should be resolved during high resolution survey by D. Chulkov et al. (2025).

Another reason for RUWE increase is a wobble of the photocenter (center of light) relative to the system’s center of mass (Z. Penoyre et al. 2020). Gaia DR3 main source catalog assumes single-star solutions (L. Lindgren et al. 2021), which are appropriate when the system’s center of mass coincides with the photocenter observed by Gaia. This condition is not met by binary systems, which causes astrometric deviations encoded in RUWE increase. The largest shift is expected for systems with periods around Gaia DR3 observational baseline of 34 months (Z. Penoyre et al. 2022), which can be noticed for spectroscopic binaries (Figure 1). RUWE excess persists both for SB1 and SB2 systems, including pairs with low secondary mass and mass ratio. A binary with equal components and $q = 1$ should be perfectly fitted by single-star model and have low RUWE.

A. Castro-Ginard et al. (2024) explored the threshold recommended to separate single objects from binary systems. It slightly varies across the Pleiades field, and a RUWE value of 1.2 is adopted as an upper limit for a reliable astrometric solution consistent with a single star model in this paper, which is stricter than the frequently used RUWE = 1.4 cutoff (C. Fabricius et al. 2021).

4.2. Forward modeling of RUWE

A. Castro-Ginard et al. (2024) further developed a forward model allowing RUWE prediction based on binary star parameters. Two obstacles arise to use it for credible investigation of sample objects. First, it was found that marginally small variation of input parameters often leads to large scatter of predicted RUWE values, which may be a model artifact. Another problem is the lack of reference objects for solid verification of model predictions. Even for SB2 binaries, an ambiguity remains, since their orbital orientation is not known, as

longitude of ascending node Ω and orbital inclination i remain undetermined (J. Southworth 2020), although the latter can be roughly estimated from Equation 2.

Simulations are carried out with *GaiaUnlimited* package (A. Castro-Ginard et al. 2024) to study the behavior of RUWE at least qualitatively. Pleiades isochrone from R. Liu et al. (2025) is used to relate stellar mass to luminosity; companions with $m_2 < 0.1M_\odot$ are considered non-luminous. The parallax is set to a sample mean of $\varpi = 7.37$ mas (Section 6.1), celestial coordinates of the cluster center are used: $\alpha = 56.74^\circ$, $\delta = 24.09^\circ$. Fixed values of apparent magnitude, mass ratio, and period are selected, eccentricity and orientation angles are distributed uniformly following the table 1 in A. Castro-Ginard et al. (2024). A total of 1000 runs were made for each combination of parameters; the median along with 0.159 and 0.841 quantile values are shown in Figure 3.

4.3. RUWE behavior

Strong dependence on binary period is predicted with a maximum around a value of 3 years due to observational time frame of Gaia DR3. While the closest systems keep a low RUWE, already at $P \sim 10$ days binarity induces RUWE excess in many simulations. Empirically for SB1 binary HII 571 with $P = 15.9$ days the RUWE value is slightly above 1.4 threshold (Figure 1). The projected decline for systems with $P \gtrsim 30$ years is largely misleading, as the model does not account for resolved binarity. Thus, V1282 Tau with an 18 year period has a $0.06''$ semimajor axis matching Gaia along-scan resolution (B. Holl et al. 2023). In practice, the resolved pairs show RUWE excess up to $2''$ separation (Figure 2).

There is a dependence on apparent magnitude as the sensitivity drops at the faint end of $G = 15$ mag, with a broad maximum around $G \sim 12$ mag. Among unresolved sources, only three have RUWE > 10, their magnitudes are within $11.9 \lesssim G \lesssim 12.9$ range (Figure 2).

The probability of detecting a companion depending on its mass ratio is of special interest. RUWE is most

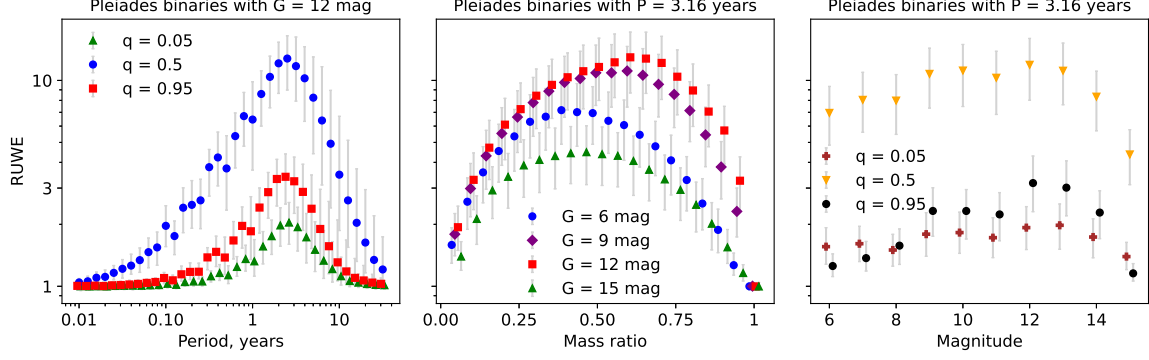


Figure 3. Prediction of RUWE values for Pleiades stars with the *GaiaUnlimited* package (A. Castro-Ginard et al. (2024), Section 4.2). The RUWE increase for marginally resolved sources that affects binaries with $P \gtrsim 20$ years is not considered.

sensitive to $q \sim 0.5$ systems. It appears that the distribution maximum is shifted toward $q > 0.5$ for $G = 9$ and 12 mag, while at the faint and bright ends it peaks at lower q (Figure 3). According to simulations, RUWE excess is noticeable at least up to $q \sim 0.03$, and the secondary masses around $0.02 M_{\odot}$, which are deep into the brown dwarf range, are detectable. The longer time coverage of Gaia DR4 hopefully will increase sensitivity and allow us to probe giant exoplanets in the Pleiades. The decrease of RUWE for binary stars with $q \sim 1$ may create a bias for member selection and multiplicity statistics in different stellar populations as discussed below.

4.4. Impact on cluster member selection

The amount of photocenter wobble relative to center of mass is smaller for binaries with $q \sim 1$, so they are more likely to have astrometric solution compatible with single star model and have a low RUWE. This effect may have broader consequences for the observed mass ratio distribution in open clusters and other stellar populations accessed with Gaia. Cluster member selection depends on many factors, such as proper motion and field stellar density, and the feasibility of credible classification varies between different stellar groups. Genuine members have a better chance to be identified if they have a reliable low-RUWE solution. Binarity introduces deviations to astrometric fit which may prevent a source from being recognized as cluster member. Objects with larger RUWE have a lower chance to be properly classified, even if no explicit cutoff is made. Thus, systems with $q \sim 1$ are more likely to get a reliable astrometric solution and to be selected as cluster members, while binaries with $q \sim 0.5$ are disfavored. A distinct peak at $q = 1$ arising during the photometric data analysis of multiplicity (A. C. Childs & A. M. Geller 2025) may be induced by the preferential selection of such near-twin binaries. The selection bias affects clusters to varying degrees and likely contributes to the large reported spread of multiplicity fraction (G. Cordoni et al. 2023).

Table 2. Gaia DR3 non-single star solutions

Source	G	RUWE	nss	SB	P	q_{ph}
Gaia DR3	mag		Type	days		
66507469798631808	6.81	0.974	SB2	2	16.7	0.40
66729880383767168	6.82	1.145	SB2	2	2.46	0.54
64898368889386624	8.12	10.395	acc9	1	953	< 0.4
65275501377570944	8.55	9.413	acc9			< 0.4
65090680344356992	9.43	6.012	Orb	2	269	< 0.4
65207709613871744	9.74	3.377	acc7	2	767	0.72
66771146429454592	10.30	1.419	SB1	1	30.2	< 0.4
65276703968959488	10.39	1.229	SB1	2	3.31	0.60
69829609819915648	10.56	9.547	tSB1	1	972	< 0.4
69883417170175488	10.63	3.223	ASB1	2	481	0.84
65232105028172160	10.64	2.921	acc7	1	2940	< 0.4
66863058730966528	10.71	1.632	acc9	1	780	< 0.4
68310359628169088	10.85	5.585	acc9	2	757	0.89
69864313155605120	11.01	1.406	SB1	1	15.9	0.48
66747816167123712	11.90	1.18	SB1	1	7.05	< 0.4
66519530066802944	12.30	2.27	acc9			< 0.4
66937859881182848	12.78	2.889	acc9	2	542	0.86
65660158649542784	12.85	13.699	acc9	1	1313	0.73
66816187748666624	12.90	14.871	ASB1	1	548	< 0.4
66944422591073024	13.31	3.381	acc9			< 0.4
64841503521468544	14.30	8.486	acc9			0.56
65229734206151680	14.78	2.622	acc7			0.61

NOTE—Complete list of nss solutions for sample objects; the nss acronyms are defined in Section 5. The SB and P columns refer to the SB1 or SB2 binarity type and period from G. Torres et al. (2021), q_{ph} is the mass ratio estimate derived from the CMD analysis (Section 6).

5. GAIA DR3 NSS SOLUTIONS

Gaia DR3 (Gaia Collaboration et al. 2023a) includes around $8 \cdot 10^5$ dedicated non-single star (nss) solutions

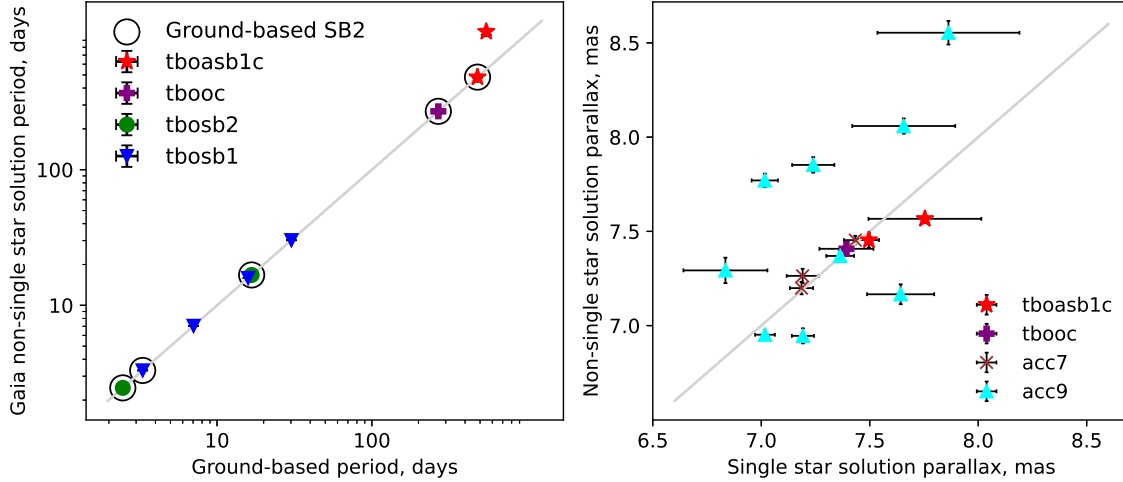


Figure 4. Left: orbital periods according to Gaia DR3 nss solutions (Section 5) and ground-based estimates from G. Torres et al. (2021). The error bars are smaller than symbol sizes. Right: parallaxes from the main source catalog and nss solutions.

representing a small fraction of the full catalog of $1.8 \cdot 10^9$ sources. Their selection function is quite sophisticated (K. El-Badry et al. 2024). Thus, face-on orbits are negatively biased (V. V. Makarov 2025). Solutions of seven different types (J.-L. Halbwachs et al. 2023; E. Gosset et al. 2025) are listed for 22 sample sources in Table 2:

- Combined astrometric + single-lined spectroscopic orbital model (*tboasb1c*, ASB1) – 2 entries.
- Orbital model for an astrometric binary with Campbell orbital elements (*tbooc*, Orb) – 1 entry
- Single-lined spectroscopic binary model – 4 entries (*tbosb1*, SB1)
- Double-lined spectroscopic binary model – 2 entries (*tbosb2*, SB2)
- Spectroscopic binaries compatible with single-lined first degree trend (*linspec1*, tSB1) – 1 entry
- Acceleration model with 7 parameters (*acceleration7*, acc7) – 3 entries
- Acceleration model with 9 parameters (*acceleration9*, acc9) – 9 entries

Among 22 entries, 17 are spectroscopic binaries from ground-based observations (G. Torres et al. 2021). For the first four types, nss solutions include orbital periods; in 8 out of 9 cases, they agree with existing estimates (Figure 4). The exception is V338 Tau ($G = 12.90$ mag), an SB1 binary with $P = 548 \pm 1$ days. Its reported period in Gaia is twice as large, $P = 1042 \pm 55$ days, which is likely an artifact of unevenly sampled data.

Astrometric solutions for 15 systems include parallaxes ϖ that account for binarity. One could expect

these values to converge better around the cluster mean of $\varpi = 7.37$ mas in comparison to single star model solutions for the same sources in the main catalog, but the results contradict this expectation. Although the reported parallax uncertainties for individual entries are smaller (Figure 4), their median ϖ differs more from the expected value and the standard deviation of the nss solutions is larger: $\varpi = 7.41 \pm 0.43$ instead of $\varpi = 7.36 \pm 0.29$ mas. The sample is small for definitive conclusions, and while the peculiar spatial distribution of these sources is possible, it seems nss solutions do not necessarily improve parallax reliability. For a larger set of triple systems, P. Nagarajan & K. El-Badry (2024) found true parallax errors are roughly ten times larger for single star solutions than for orbital nss solutions, and five times larger than for acceleration solutions.

Four entries have masses of both components derived in Gaia DR3 (Gaia Collaboration et al. 2023b). The mass ratios obtained for sources with combined astrometric and SB1 solutions (*tboasb1c*) contradict the existing estimates. The reported mass ratio for HII 173 in Gaia DR3, $q \sim 0.52$, is refuted by the $q \sim 0.95$ estimate for a known SB2 system (Table 1). For SB1 binary V338 Tau, the nss solution infers $q \sim 0.86$, while $q < 0.4$ is expected from the multicolor photometry (Section 6).

Inclination estimates from Equation 2 for the two SB2 systems roughly agree with nss solutions. HD 23158 has an orbital solution with $i = 109 \pm 1^\circ$ ($\sin i \sim 0.95$), while Equation 2 suggests an edge-on orbit with $\sin i \sim 1.00$. For HII 173 with *tboasb1c* type, Gaia provides $i = 86 \pm 2^\circ$ ($\sin i \sim 1.00$) versus $\sin i = 0.97$ value from Equation 2.

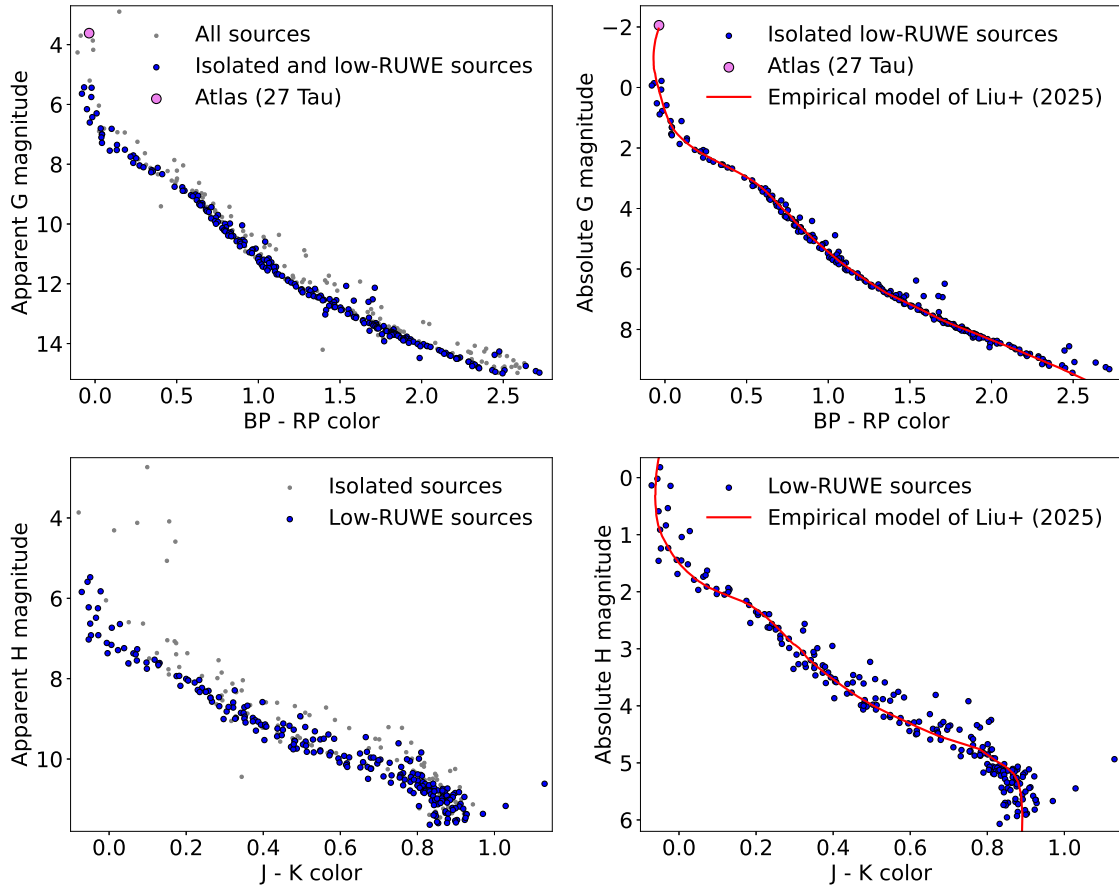


Figure 5. Pleiades stars in the CMD using Gaia (top) and 2MASS (bottom) photometric data. Apparent and absolute magnitudes are shown in the left and right panels, respectively. Extinction correction is applied to the model curves when deriving absolute magnitudes. Isolated sources are defined as those with a single Gaia counterpart within $4''$. A separate threshold of $\text{RUWE} < 1.2$ is adopted (Section 6.1). For Atlas, a distance estimate of 136.2 pc is used (G. Torres et al. 2025).

6. COLOR-MAGNITUDE DIAGRAM ANALYSIS

Pleiades is a typical example of a coeval simple stellar population that shares a common age, metallicity and remains relatively compact in its central part. As a result, cluster members have distinct mass-magnitude and color-magnitude relations (Figure 5). The analysis of the color-magnitude diagram (CMD) is a long-standing way of cluster characterization, enabling the study of its multiplicity properties, as binaries with large enough secondary flux show an offset relative to the single stars sequence (C. Betts 1975). High-quality Gaia photometric data in G , BP and RP passbands (M. Riello et al. 2021) are widely used to put constraints on binary population within open clusters (G. Cordoni et al. 2023).

The sensitivity of the photometric method depends on the component mass ratio, while being independent of the orbit’s size and orientation for unresolved sources. It becomes progressively less reliable for low-mass companions as secondary component flux becomes harder to

observe in front of a primary star. This section explores an application of the CMD analysis to the Pleiades.

A subsample of sources with reliable astrometric and multicolor photometric data is defined in Section 6.1 and used to adopt a single-star isochrone and estimate mass ratio in Section 6.2. The results are validated for known spectroscopic systems in Section 6.3. The CMD analysis has its caveats and outlier sources are discussed in Section 6.4. Differential interstellar extinction is proposed to cause the discrepancies in Section 6.5. An area of enlarged extinction which biases the derived binary properties is outlined in Section 6.6. Finally, the revealed binary star candidates are presented in Section 6.7.

6.1. Subsample with reliable Gaia data

Besides multiplicity, several factors affect the source’s position in the CMD. One is purely geometrical. The tidal radius of Pleiades (~ 13 pc, J. D. Adams et al. (2001)) is of the order of one-tenth the distance to the Sun. This causes a sizable scatter in the CMD due to

variations in individual stellar distances. Accurate parallax (ϖ) estimation enables tackling this problem by switching from apparent (G) to absolute magnitude:

$$G_{\text{abs}}^* = G + 5 \log \varpi - 10 \quad (3)$$

where ϖ is measured in mas (10^{-3} arcsec). Note that here G_{abs}^* is uncorrected for interstellar extinction, as absorption is instead taken into account in model isochrones. Similar conversion can be applied to arbitrary passbands. However, reliable parallaxes are not available for every star in Gaia DR3, and the appropriate subsample is defined by two separate conditions:

- Sources with $\text{RUWE} < 1.2$ are selected, as larger values may indicate the presence of a companion (Section 4) which can disturb parallax estimation.
- Entries with another Gaia DR3 source within $4''$ radius are excluded to avoid flux contamination from a nearby star in the BP and RP passbands.

These criteria are met by 231 sources shown with blue dots in the CMD (Figure 5). The median of the reported parallax uncertainties σ_{ϖ}/ϖ is 0.26%, and the precision of absolute magnitude calculation through Equation 3 is less than 0.01 mag for 94% of entries. The median distance, estimated as $1/\varpi$, is 135.6 pc for this subsample; the 0.159 and 0.841 quantile values are 133.7 and 138.5 pc, respectively. These distances serve as references for sources with unreliable astrometric solutions.

Importantly, binaries are not wiped out from this subsample completely, as some low-period ($P \lesssim 30$ days) systems show small RUWE values (Figure 1). The seven brightest stars with $G < 5.4$ mag are missing from the subsample due to RUWE excess or a two-parameter solution in the case of Alcyone (25 Tau). Their absence is a disadvantage for isochrone fitting. Fortunately, the second-brightest Pleiades member, Atlas (27 Tau), is observed as a spectroscopic and interferometric binary, which allowed G. Torres et al. (2025) to derive a 136.2 ± 1.4 pc distance from the orbital solution alone. Hence, its absolute magnitude is reliable. Due to their weak dependence on color, high-mass binaries are almost indistinguishable from single stars in the CMD (Figure 6), hindering detection of their multiplicity.

6.2. Binary stars in the CMD

For coeval main sequence stars, an absolute magnitude directly relates to mass. Theoretical isochrones such as PARSEC (A. Bressan et al. 2012; C. T. Nguyen et al. 2022) or MIST (J. Choi et al. 2016) are widely used to reproduce the observed color-magnitude relation and fit the cluster’s age or multiplicity fraction. F.

Wang et al. (2025) compared the observed sequences in Pleiades, Hyades, and Praesepe with theoretical models and found similar deviation trends for these open clusters. The proposed $BP - RP$ color correction reaches its maximum of 0.25 and 0.15 mag for MIST and PARSEC models, respectively, in the $0.3 - 0.5 M_{\odot}$ range. R. Liu et al. (2025) adjusted an empirical model using Gaia and 2MASS (M. F. Skrutskie et al. 2006) photometric data for Pleiades. It closely matches the subsample stars (Figure 5) and was adopted for further calculations.

The ultimate goal is to test if the observed photometric data are consistent with a single star, and if not, to estimate stellar masses and mass ratio. Table 3 from R. Liu et al. (2025) provides an empirical mass – absolute magnitude relation for single Pleiades stars. For unresolved binary systems, the total flux is considered to be a sum of primary and secondary component fluxes. Therefore, the combined magnitude is derived as:

$$G = -2.5 \log(10^{-0.4G_1} + 10^{-0.4G_2}) \quad (4)$$

where G_1 and G_2 are component magnitudes. Here it is assumed that both stars evolve as single ones depending on their masses m_1 and m_2 . This approach may be incorrect for very close binaries, if the components have undergone mass transfer, which should be rare in a relatively young cluster. The synthetic magnitudes in Gaia and 2MASS passbands are calculated for a dense grid of masses in the $0.1 M_{\odot} < m_1 < 4.9 M_{\odot}$ range with a $0.001 M_{\odot}$ step. Mass ratios $q = m_2/m_1 \leq 1$ are sampled at 0.001 intervals. Their range depends on m_1 , since the $m_2 \geq 0.1 M_{\odot}$ condition should be met. The observational sample includes $m_1 \gtrsim 0.5 M_{\odot}$ stars; therefore, substellar objects with $m_2 \lesssim 0.1 M_{\odot}$ can be neglected.

For sources with $\text{RUWE} < 1.2$, astrometric data should be reliable and absolute magnitudes are derived from the reported Gaia DR3 parallaxes using Equation 3. The nominal uncertainties σ_{ϖ} are used to calculate the inferred magnitude bounds assuming $\varpi \pm \sigma_{\varpi}$ parallax values. For other entries, a standard distance of 135.6 pc is adopted, which is a median for the low-RUWE subsample (Section 6.1), while values of 133.7 and 138.5 pc constrain the error range. As shown by the example of Atlas with $\text{RUWE} = 4.117$, the reported parallax can be misleading, and the cluster average better reflects its true distance. The $1/\varpi$ estimate from $\varpi = 8.12 \pm 0.48$ mas is around 123 pc; however, the orbital solution from G. Torres et al. (2025) securely puts Atlas inside the cluster’s core with a 136.2 ± 1.4 pc value.

Differences between the observed (G , BP and RP) and modeled (\hat{G} , \hat{BP} and \hat{RP}) magnitudes are calculated with Equation 5. The minimum photometric residual χ is selected to define a synthetic binary which has

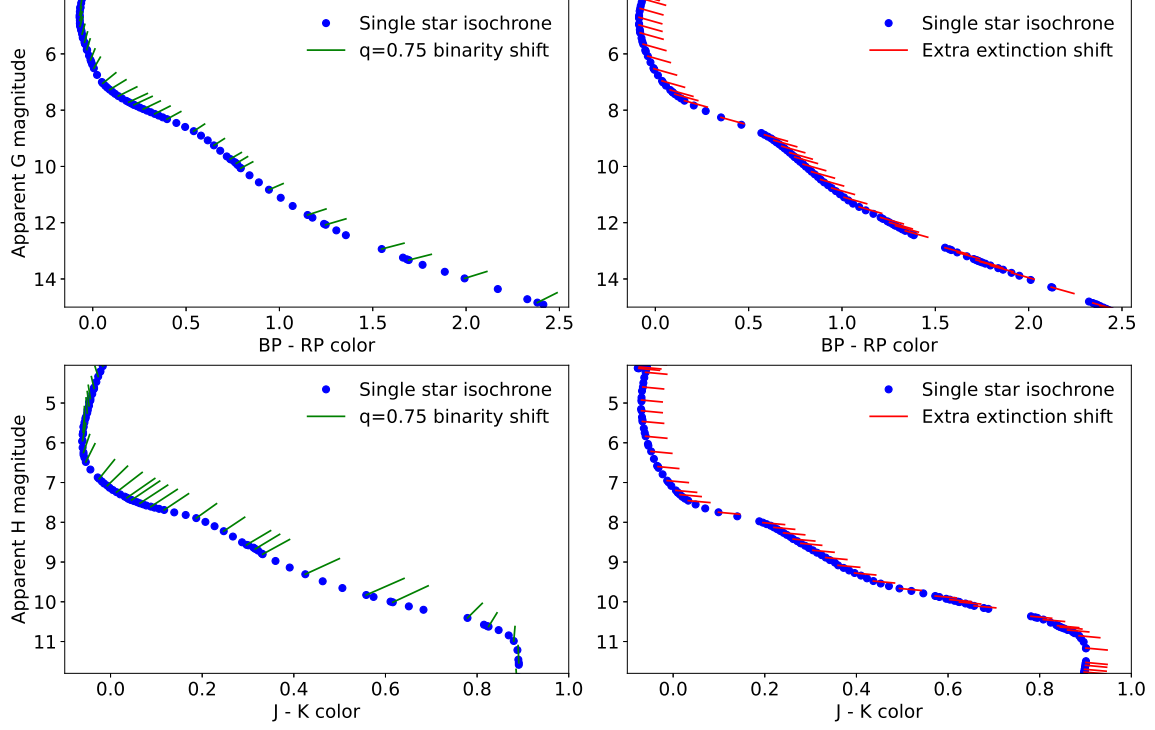


Figure 6. Left: shift of binary systems with $q = 0.75$ in the CMD relative to the single star sequence of R. Liu et al. (2025). For twin binaries ($q = 1$), the color index is unchanged and the combined magnitude becomes brighter by 0.75 mag. Right: impact of enlarged absorption ($A_V = 0.5$ relative to $A_V = 0.23$ mag) on PARSEC 2.0 isochrones with star-by-star derived extinction (J. A. Cardelli et al. 1989; J. E. O’Donnell 1994), calculated via the CMD 3.8 interface (<http://stev.oapd.inaf.it/cmd>), $R_V = 3.1$.

the closest match with the observed photometric data for sample objects. Similar calculations are made for the 2MASS photometric system in J , H and K bands.

$$\chi = \sqrt{(G - \hat{G})^2 + (BP - \hat{BP})^2 + (RP - \hat{RP})^2} \quad (5)$$

For sources near the empirical single-star isochrone, Equation 5 minimization favors solutions with $q < 0.4$ as expected. These entries are considered indistinguishable from single stars based on Gaia photometry. Out of 231 isolated low-RUWE sources, a $q > 0.4$ solution is preferred for 35 entries and $q > 0.5$ for only 20 (8.7%) of them. Of these, just five systems are known as spectroscopic binaries (Section 3). The value of photometric residual χ is within 0.006 mag for all but four of the entries with $q > 0.4$; this is likely a consequence of increased extinction in a relatively small cluster area (Section 6.4, Figure 7). The median residual is almost eight times larger if 2MASS photometry is adopted instead of Gaia for the same group of 35 objects. The lower accuracy limits its relevance for binarity parameter estimation, and only Gaia photometry is further considered.

6.2.1. Resolved systems

An important precaution concerns binaries in the $0.1 \lesssim \rho \lesssim 2$ arcsec separation range as they are effec-

tively in the semiresolved regime in Gaia DR3. Depending on separation, their reported G magnitudes can be related to a sole star, while BP and RP fluxes are combined from both components. Moreover, BP and RP fluxes can be affected at larger distances in the vicinity of a bright neighbor. Consequently, such systems appear as outliers in color-color diagram (D. Chulkov 2024), and the straightforward use of Equation 5 brings an incorrect result. Mass ratios of the resolved systems are estimated in D. Chulkov et al. (2025). For nine sample entries, BP and RP magnitudes are not available due to interference from another Gaia source within $4''$.

6.3. Validation for SB2 systems

Double-lined spectroscopic (SB2) binaries with orbital solutions listed in Table 1 serve for validation of photometrically estimated q_{ph} (Figure 8). Based on 16 entries, it is lower than the spectroscopic value by $\Delta q = q_{sp} - q_{ph} = 0.09 \pm 0.12$, in line with the $\Delta q = 0.1$ mean offset from R. Liu et al. (2025) (figure 8 in the respective paper), who used a Bayesian framework to derive mass ratios for the Pleiades stars based on Gaia and 2MASS data. Despite the similar result, our samples are different, and among the entries appearing in both, only HD 23631B ($G = 9.74$ mag) shows closer agreement in the R. Liu et al. (2025) work. For this star, a brighter

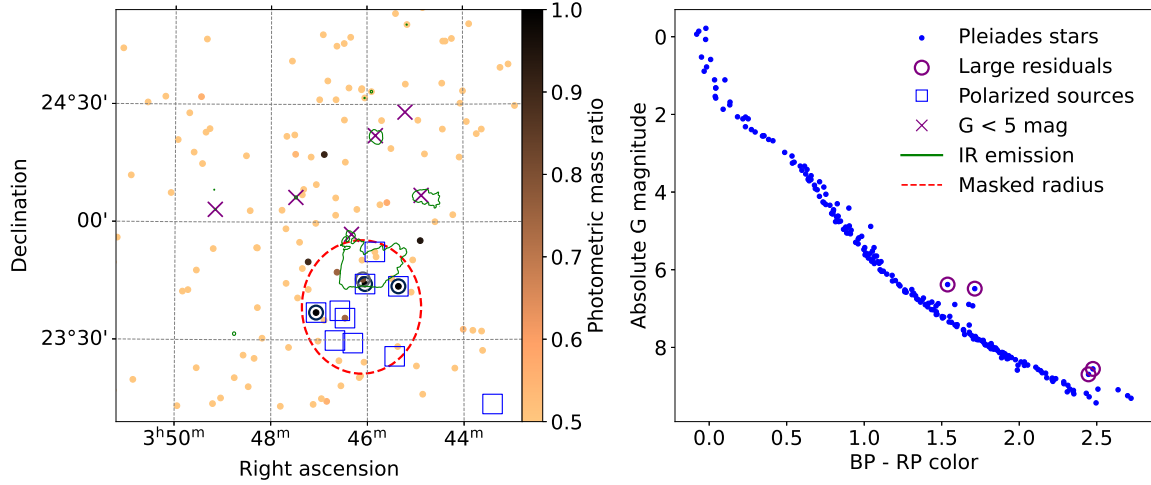


Figure 7. Sky map of Pleiades stars with reliable astrometric and photometric data; the central part of the considered two degree radius is shown. Photometric mass ratio (Section 6.2) is color-coded, darker shades correspond to larger q . The four entries that are poorly fitted by either single-star or binary-star models (Section 6.4) are encircled; these are shown in the CMD (right panel). The six brightest Pleiades members are marked with purple crosses for guidance. Stars with linear polarization above 1% threshold according to M. Breger (1986) are enclosed in blue boxes; this includes sources with large RUWE. Nebulosity observed in the WISE W4 passband ($22 \mu\text{m}$, E. L. Wright et al. (2010)) is recovered using the HiPS2FITS service and shown with a green curve. A red circle encompasses the area of unreliable photometric q estimation due to enlarged extinction (Section 6.6).

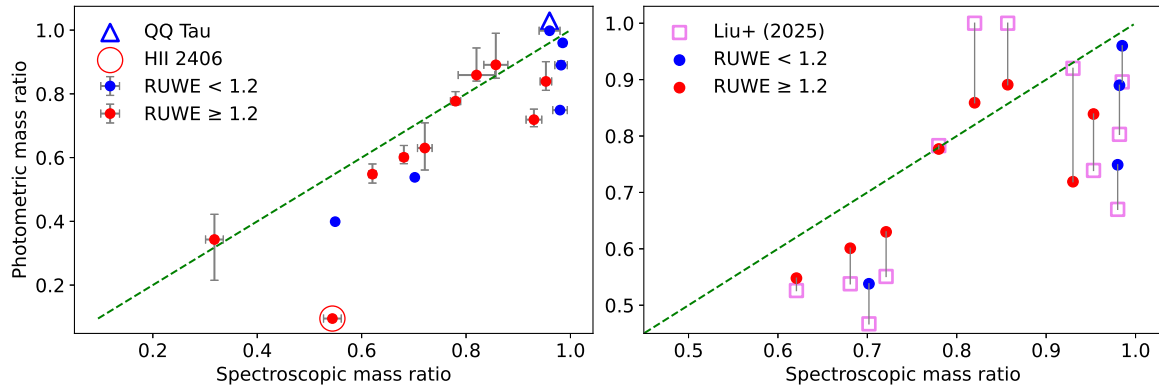


Figure 8. The mass ratios of SB2 binaries (Table 1) derived from the orbital solutions and CMD analysis. The diagonal line indicates the agreement of estimates. The error bars of photometric mass ratio account only for distance uncertainty; values of $q \lesssim 0.5$ have particularly low credibility. For QQ Tau, an enlarged extinction assumption is required to explain the photometric data (Section 6.4.1). The right panel shows a comparison with the best-fit result from R. Liu et al. (2025) photometric analysis.

neighbor ($G = 7.29 \text{ mag}$) at $\rho = 6.3''$ could slightly affect BP and RP reported fluxes. For another 11 entries, the results are similar or the estimate from this study has better agreement with spectroscopic data (Figure 8).

An example of HII 2406 with $q_{\text{sp}} \sim 0.54$ indicates the limitation of photometric binary inference. G. Torres et al. (2021) spectroscopically measured the flux ratio of $1.3 \pm 0.3\%$; however, its binarity is not recovered photometrically, including in the study by R. Liu et al. (2025). Sources with $q_{\text{sp}} > 0.6$ start to reveal themselves as binary stars, albeit with an underestimated q_{ph} value.

A difference between spectroscopic and photometrically fitted q persists in other clusters. A. C. Childs

et al. (2024) obtained $\Delta q = q_{\text{sp}} - q_{\text{ph}} = 0.13$ mean underestimation and adopted $\Delta q = 0.2$ as effective uncertainty (figure 10 in the respective paper). The recovered mass ratio is also underestimated relative to a true one in simulations modeling the photometric behavior of unresolved binaries (figure 5 in A. L. Wallace (2024)). Notably sequences for binary systems with $q = 0.9$ and $q = 1$ almost coincide in the CMD leading to degeneracy for near-twin pairs (figure 5 in Y. Jiang et al. (2024)).

6.4. Sources with large photometric residuals

Four low-RUWE sources clearly appear above the single-star sequence (Figure 7), yet their residual in

Equation 5 is larger than 0.01 mag, indicating that binary star models poorly fit them. The outlier objects can be interpreted as triple stars. Indeed, A. A. Malofeeva et al. (2023) estimated no less than 10% of non-single Pleiades stars are triple or quadruple. However, this explanation can be challenged by a combination of two factors: these sources have low RUWE and are located in a small area reported for excessive absorption.

Based on the dynamical stability criterion of triple systems (R. A. Mardling & S. J. Aarseth 2001), the outer period should be larger than the inner one at least by a factor of 4.7 (A. Tokovinin 2021). As evident from empirical data (Figure 1) and simulations (Section 4.3), binaries with $P \gtrsim 20$ days start to show RUWE excess. The inner orbit therefore should be very compact to meet the stability criterion and keep the RUWE low.

6.4.1. QQ Tau

The discussion on specific objects begins with QQ Tau ($G = 14.26$ mag), a known SB2 system with near-twin components and 2.46 days period (A. Frasca et al. 2025). Its photometric residual, $\chi = 0.03$ mag (Equation 5), is at least five times larger than for the vast majority of sources. Three possible explanations can be mentioned. One requires flux from a tertiary component. To meet dynamical stability constraints and simultaneously keep a low RUWE value (1.12), the outer period should be roughly within 12 – 20 days, making this system a convenient target for follow-up spectroscopic observations.

Another option is that isochrones designed for single stars are inadequate for short-period binary components. There are three more SB2 systems (V1229 Tau, HII 761 and V888 Tau) with periods within 3.5 days (Table 1), their photometrically fitted q is underestimated compared to the spectroscopic q following a general trend (Figure 8). Due to combination of low mass and period, QQ Tau has the smallest orbit size among them.

The final and indeed the favored possibility is an extinction excess toward QQ Tau affecting the photometric q estimation. This suggestion is justified by the observed linear polarization of QQ Tau and the other stars in the vicinity (Figure 7) discussed in Section 6.5.

6.4.2. Other outlying sources

The largest photometric residual (Equation 5), $\chi = 0.13$ mag, belongs to HII 870 ($G = 12.13$ mag), which has a reliable astrometric solution with $\text{RUWE} = 1.095$. Its proper motion, parallax, and radial velocity from Gaia and ground-based observations are consistent with cluster membership. J. Bouvier et al. (1997) detected a faint companion at $\rho = 0.5''$ with $\Delta J = 4.4$ mag and estimated $q = 0.24$. Whether it is a physical or optical pair, this component's luminosity

is negligible. Companions with a noticeable flux in the 880 nm passband are ruled out for $\rho > 0.1''$ separations by speckle observations (D. Chulkov et al. 2025).

V811 Tau appears within $10'$ from the previous source, has exactly the same RUWE and a similar magnitude of $G = 12.07$ mag, while its photometric residual, $\chi = 0.03$ mag, is smaller. Unlike for HII 870, the large uncertainties of radial velocity measurements from LAMOST (A. Frasca et al. 2025) and SDSS (S. Mészáros et al. 2025) allow to suggest this star is not single.

2MASS J03460556+2345261 is a fainter star with $G = 14.38$ mag located just $1.4'$ from HII 870. Its photometric residual of $\chi = 0.01$ mag is moderate, however the shift in the CMD due to enlarged extinction is less prominent for faint objects at optical wavelengths (Figure 6). It has a large $J - K = 1.13$ mag value (Figure 5) which is a sign of large extinction rather than binarity.

HII 975 ($G = 10.36$ mag) has a RUWE of 1.311 which is slightly above the threshold for reliable solution. This source has a large $\chi \sim 0.08 - 0.09$ mag residual regardless of whether the reported Gaia DR3 parallax or the cluster mean distance is adopted for absolute magnitude calculation. Along with QQ Tau, HII 870, and V811 Tau, HII 975 shows a polarization excess, discussed below.

6.5. Extinction and polarization

Interstellar extinction and reddening is a complex and often overlooked factor (J. Maíz Apellániz 2024). The extinction in a given passband depends both on the interstellar matter along the line of view and the source energy distribution, and affects stars of different temperatures differently. Due to proximity to the Sun and moderate galactic latitude ($b \sim -24^\circ$), Pleiades stars have a low extinction with $A_V \sim 0.1 - 0.15$ mag (T. J. David & L. A. Hillenbrand 2015). The fiducial PARSEC model used by R. Liu et al. (2025) adopts $A_V = 0.135$ mag.

The extinction and reddening within the Pleiades is not uniform. Unrecognized differential extinction can be misinterpreted as the outcome of stellar multiplicity during CMD analysis (B. J. Taylor 2008). Several works attempting to derive reddening values for millions of stars are summarized in the SDSS 19 *astralMWMLite* catalog (SDSS Collaboration et al. 2025). The results for the sample objects are contradictory and appear to have limited credibility for comparison between cluster members. For instance, for HD 23512, the reported values of color excess $E(B - V)$ are between 0.04 and 0.86 mag.

Unlike extinction or reddening, polarization is directly measured and can be used to trace the absorption. Linear polarization occurs when light experiences nonuniform dichroic absorption by aligned asymmetric dust particles (N. V. Voshchinnikov 2012; B. G. Andersson

et al. 2015). It is loosely correlated with total extinction, the upper bound of the polarization fraction is around 3% per one magnitude of A_V (K. Serkowski et al. 1975). M. Breger (1986) conveyed a large polarimetric survey of Pleiades and found a linear polarization fraction above 1% for 10 sources, all located to the south of Merope star (Figure 7). A larger than average extinction is expected for these objects. All stars with large photometric residual discussed in Section 6.4 show a polarization excess, apart from 2MASS J03460556+2345261 with no data.

HD 23512 ($G = 8.04$ mag) is the only sample source with $G < 10$ mag and a large polarization, it is considered a standard star (J. C. Hsu & M. Breger 1982). D. V. Cotton et al. (2024) argued its polarization may be caused by a yet unconfirmed companion. Indeed, the large RUWE value of 4.28 leaves little doubt this star is not single. However, considering that neighboring sources also show large polarization, enlarged absorption by the interstellar medium seems a more plausible interpretation. E. L. Fitzpatrick & D. Massa (2007) studied spectral energy distribution for this object from ultraviolet to infrared and derived color excess $E(B - V) = 0.36 \pm 0.01$ mag with $R_V = 3.2 \pm 0.2$, which suggests total extinction A_V around 1 mag. However, an unaccounted companion could compromise this result.

6.6. Excluded region

Stars with large observed polarization and, hence, extinction may have biased binary parameters estimates. Considering these sources are located in a relatively small region (Figure 7), it is convenient to separate them from other cluster members. A radius of $17'$ around celestial coordinates $\alpha = 56.53^\circ$, $\delta = 23.64^\circ$ defines a problematic area. Diffuse WISE W4 $22 \mu\text{m}$ emission (E. L. Wright et al. 2010) partially overlaps with this region.

The designated area is outside of the cluster core and should not have peculiar multiplicity properties. It includes 26 Gaia DR3 sources; 17 (65%) of them have no close neighbors and $\text{RUWE} < 1.2$ (Section 6.1). The corresponding numbers for the remaining cluster part are 384 and 214, yielding a proportion of 56%. Among low-RUWE isolated sources, the fraction of entries with large photometrically inferred mass ratio is drastically different within and outside of the discussed area. For six out of 17 entries (35%) inside the radius, $q_{\text{ph}} > 0.6$ is favored. The corresponding fraction outside is six out of 214 (2.8%). Such a difference indicates that extinction excess has contaminated q_{ph} estimates, and the affected 26 sources are excluded from further statistical analysis.

6.7. Binary stars candidates

The binary candidates inferred from the CMD analysis are shown in Figure 9. A visible excess of binaries at the

faint end of the sample is caused by the truncation bias. For single stars the $G = 15$ mag threshold corresponds to $0.5 M_\odot$, and the less massive stars miss the sample. However, unresolved binaries with the primary masses up to $m_1 \sim 0.42 M_\odot$ may reach the limiting magnitude.

For the most massive stars, the impact of binarity is hardly noticeable both in the visible and infrared colors (Figure 6) and the results for the six brightest members with $G < 5$ mag are spurious, even though they are reasonably close to the spectroscopically derived value for Atlas (Table 1). The photometrically inferred binarity with $q \sim 0.63$ for Pleione (28 Tau, $G = 5.20$ mag) can also be an artifact. This is a known SB1 system with $q < 0.2$ (J. Nemravová et al. 2010). The existence of another companion was proposed, but numerous searches have not succeeded so far (R. Klement et al. 2024).

The inferred mass ratios for unresolved sources are plotted in Figure 10. The errors shown account only for distance uncertainties, while the full uncertainties reach at least $\Delta q \sim 0.1$ (Section 6.3). For SB2 binaries with orbital solutions (Table 1), the spectroscopic q is more accurate and used instead of the photometrically derived value. The latter is particularly model-dependent for high-RUWE sources, and becomes incorrect if a given object is outside the $133.7 - 138.5$ pc distance range.

7. BINARITY CENSUS

7.1. Sample definition

Census of binaries in the Pleiades requires both resolved and unresolved systems to be counted. Pairs with $0.1 \lesssim \rho \lesssim 2$ arcsec separation are semiresolved in Gaia DR3, and standard procedures for photometric q estimation should not be applied for them (Section 6.2.1). The resolved systems are divided into two classes depending on whether Gaia DR3 has separate entries for both components. The mass ratio is estimated from the reported G_1 and G_2 magnitudes or flux contrast measured in speckle observations when G_2 is unavailable.

At least 16 multiple systems with three or more components are identified in the sample. All of them include resolved companions; their configurations and parameters are discussed in the Appendix of D. Chulkov et al. (2025). For the binary fraction estimate, each system is counted only once. Hierarchical triple systems consist of an inner pair with stars Aa and Ab, and an outer component B (occasionally, star B is more massive than the inner pair components). Mass ratios of Aa - Ab and Aa - B pairs are compared, and the larger one is selected for statistics. If both inner pair components have masses below the $0.5 M_\odot$ threshold, then the outer q is considered. An unknown third component is possible in presumed binary systems and may disturb q estimation.

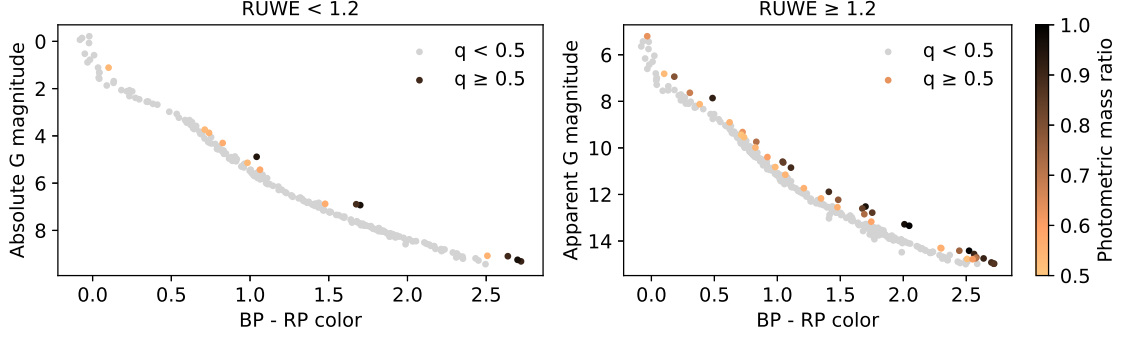


Figure 9. Binary star candidates inferred from the CMD analysis; sources with resolved companions within $4''$ are excluded (D. Chulkov et al. 2025). The entries with low and high RUWE are considered in the left and right panels, respectively.

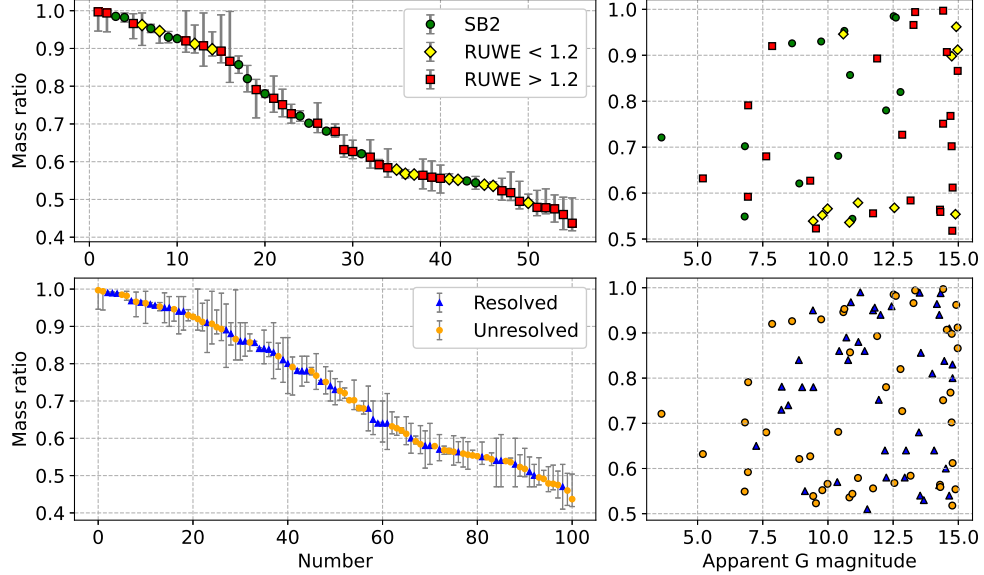


Figure 10. The estimated mass ratios for unresolved binaries (top panel) and the whole binary population (bottom panel).

The input list of cluster members includes 410 Gaia DR3 entries (Section 2); 20 of them are deemed secondary components within Gaia-resolved systems, reducing the number of unique systems to 390. After omitting objects from the area of high extinction (Section 6.6), 364 sources remain. Finally, 16 systems with $m_1 < 0.5M_\odot$ are exempted from the binary fraction calculation to eliminate the truncation bias, leaving 348 entries, listed with their adopted mass ratios in Table 4.

7.2. Binary fraction

In the resolved multiplicity survey (D. Chulkov et al. 2025) the binary fraction $f = 6.7\%_{-0}^{+1.8}$ for $q > 0.6$ systems or $f = 9.8\%_{-1.0}^{+0.3}$ for $q > 0.5$ within the 27 – 1350 au projected separation range was obtained. Un-

der crude assumptions it was extrapolated to $f \sim 17\%$ for $q > 0.6$ or $f \sim 25\%$ for $q > 0.5$ binaries across all orbit sizes. Following this study, more robust constraints can be placed. Summing up the resolved and unresolved systems, 57_{-2}^{+9} binaries with $q > 0.6$ are counted, corresponding to $f = 16.4\%_{-0.6}^{+2.6}$ fraction, or 81_{-5}^{+7} for $q > 0.5$, yielding $f = 23.3\%_{-1.5}^{+2.0}$ for cluster members with $m_1 > 0.5M_\odot$. These align with the prior estimates.

Photometric q can be underestimated up to $\Delta q \sim 0.1$ (Section 6.3). The less severe bias exists for speckle observations (section 6.2 in D. Chulkov et al. (2025)). No corrections were applied, so the estimated binary fraction may represent the lower bound of the real value.

Table 3. Pleiades binary fraction in the literature

q_{\min}	m_1	f	Ref	f , this study
	M_{\odot}	%		%
–	0.11 – 4.90	34 ± 2	L25	> 41 ($m_1 > 0.5M_{\odot}$)
–	$\sim 0.5 - 5$	> 57	T21	> 41
–	0.57 – 3.75	41 ± 4	N20	> 40
–	0.57 – 3.75	54 ± 4	L25	
–	0.5 – 1.8	73 ± 3	M23	> 41
–	0.50 – 0.90	45 ± 5	L25	> 37
–	0.90 – 1.60	55 ± 7	L25	> 47
0.4	0.5 – 1.2	19 ± 1	P23	23 ($q > 0.5$)
0.5	0.28 – 3.19	13	J24	23 ($m_1 > 0.5M_{\odot}$)
0.5	0.24 – 1.66	17 ± 2	A25	24 ($m_1 > 0.5M_{\odot}$)
0.5	0.6 – 1.0	23 ± 6	P03	23 ± 3
0.5	0.6 – 1.0	20 ± 3	N20	
0.5	0.6 – 1.0	22 ± 4	L25	
0.6	0.1 – 5	22 ± 4	L23	16 ($m_1 > 0.5M_{\odot}$)
0.6	0.18 – 2.30	9 ± 1	D23	17 ($m_1 > 0.5M_{\odot}$)
0.6	0.18 – 2.30	11 ± 1	L25	
0.6	0.24 – 1.66	13 ± 2	A25	17 ($m_1 > 0.5M_{\odot}$)
0.6	0.4 – 3.6	14 ± 2	J21	16 ($m_1 > 0.5M_{\odot}$)
0.6	0.4 – 3.6	12 ± 2	L25	
0.6	0.6 – 0.9	10 ± 3	J21	14 ± 2
0.6	0.9 – 1.2	15 ± 4	J21	15 ± 1

NOTE—Selected binary fraction estimates for the Pleiades compared with the present study. The lower limit on f is given if authors adopt no cutoff on q . References: A25 – J. S. Alexander & M. D. Albrow (2025), D23 – J. Donada et al. (2023), J21 – V. V. Jadhav et al. (2021), J24 – Y. Jiang et al. (2024), L23 – L. Long et al. (2023), L25 – R. Liu et al. (2025), M23 – A. A. Malofeeva et al. (2023), N20 – H. Niu et al. (2020), P03 – D. J. Pinfield et al. (2003), P23 – X. Pang et al. (2023), T21 – G. Torres et al. (2021).

7.3. Comparison with other works

Several estimates of binary fraction in the literature are listed in Table 3 with an emphasis on recent results relying on Gaia DR3 data. Most of them cover a large number of clusters, while this study focuses on the Pleiades, allowing its in-depth investigation starting from the member selection in D. Chulkov (2024). The binary fraction in the 0.6 – 1.0 M_{\odot} mass range, $f = 23.4^{+2.5}_{-1.9}$ for $q > 0.5$, perfectly agrees with the earlier $f = 23 \pm 6\%$ value of D. J. Pinfield et al. (2003).

Contrary to clusters, there are few recent binarity estimates for the field stars. The field population is complicated by diverse ages and has a significant contribution from systems with white dwarfs, which requires

model-dependent bias corrections. For the F, G, and K-type stars, M. Reggiani & M. R. Meyer (2013) obtained $f = 17 \pm 3\%$ for $q > 0.6$, which aligns with $f = 15.3^{+1.7}_{-0.5}$ binary fraction among 0.6 – 1.5 M_{\odot} Pleiades stars.

This study does not consider $G > 15$ mag sources ($M \lesssim 0.5M_{\odot}$), as their member selection is obstructed by the lack of radial velocity data. Since many authors include low-mass stars in the statistics, direct comparison is impeded. The literature estimates (Table 3) are typically lower than in this study, possibly due to two factors. First, here the resolved binary population was separately considered, which makes an essential contribution for the nearby cluster. Another reason is a preferential loss of binary stars during membership classification due to less reliable astrometric solutions in Gaia. A remarkable exception is the $f = 22 \pm 4\%$ estimate from L. Long et al. (2023). It appears to include entries with photometric $q > 0.6$ along with spectroscopic binaries and high-RUWE sources, many of which are below this threshold, thus yielding a relatively large value.

7.4. Mass dependence and mass ratio distribution

While the binary fraction of resolved systems was found to be distributed rather evenly over the magnitude bins, the unresolved sources produce a subtle minimum for solar-mass stars in Figure 11. According to table 6 from R. Liu et al. (2025), the binary fraction in the Pleiades does not change with primary mass in the 0.5 – 3 M_{\odot} range for $q > 0.3$ systems, set at $f \sim 30\%$. In figure 9 of V. V. Jadhav et al. (2021), the binary fraction for $q > 0.6$ binaries reaches a maximum of around 30% at 1.5 M_{\odot} and drops abruptly for less massive stars. In the field, the multiplicity fraction increases with stellar mass (S. S. R. Offner et al. 2023). However, N. Susemihl & M. R. Meyer (2022) concluded that it is more universal when a $q > 0.6$ mass ratio cutoff is taken.

The mass ratio shows hints of a bimodal distribution with a dip around $q \sim 0.7$ in Figure 11. It resembles the curve in figure 12 from R. Liu et al. (2025) where the breakpoint was found at slightly larger $q = 0.79 \pm 0.05$. A similar trend is seen for Pleiades and a few other clusters in figure 3 of J. S. Alexander & M. D. Albrow (2025), where it was interpreted as a data reduction artifact. There is little agreement with figure 15 in G. Torres et al. (2021), and the latter histogram is more consistent with a flat distribution. The obtained results contradict the decreasing function in figure 4 of A. A. Malofeeva et al. (2023). Star formation simulations from a giant molecular cloud by C. Cournoyer-Cloutier et al. (2024) show in figure 5 that mass ratio distribution forms a subtle minimum around $q \sim 0.7$ relative to the primordial population during the process of cluster assembly. For

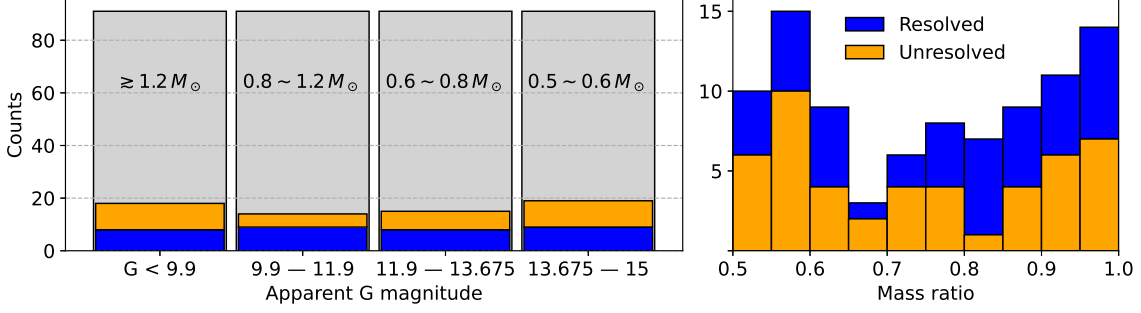


Figure 11. Left: number of resolved and unresolved binaries with $q > 0.6$ depending on source apparent magnitude. Approximate mass ranges for single stars are shown. Right: mass ratio distribution for binary stars with $q > 0.5$ in the Pleiades.

comparison, the observed mass ratio distribution in the field is considered flat in the $0.2 < q < 0.95$ range with a peak for twin binaries (D. Raghavan et al. 2010).

7.5. Low-luminous companions

A mass ratio cutoff was applied previously to select systems with significant secondary flux. With some caveats, it is possible to extend the survey toward less luminous companions. Throughout this study, only main sequence stars were considered. Three white dwarfs are possibly related to Pleiades (J. Heyl et al. 2022). The presence of binary systems with white dwarfs is proposed (S. M. Grondin et al. 2024), yet none of the candidates is conclusively confirmed. If existent, a degenerate star was once the more massive component in the pair.

Entries with photometric $q \leq 0.5$ are considered indistinguishable from single stars (Figure 9), and parameter RUWE (Section 4) becomes the main binarity indicator in the low q range. There are 40 ± 5 sources ($f = 11.5 \pm 1.4\%$) with inferred $q \leq 0.5$ and RUWE value above 1.4. If a less stringent RUWE > 1.25 threshold is used, this number increases to 54^{+5}_{-6} ($f = 15.5\%^{+1.5}_{-1.7}$). As discussed in Section 4.3, RUWE is presumably sensitive enough to astrometric deviations from some brown dwarfs, but not giant planets at the Pleiades distance.

Additionally, there are few confirmed binaries with low photometric q and RUWE. These include two SB1 binaries, two speckle-resolved pairs with $\rho < 1''$ and five wider Gaia-resolved pairs with RUWE of primary component below 1.25. Overall, the binary fraction in the $q \leq 0.5$ range is no less than $14.9 \pm 1.5\%$ adopting RUWE > 1.4 threshold or $18.1\%^{+1.4}_{-1.7}$ for RUWE > 1.25 .

Summing up all suspected binaries, the lower limit on total binary fraction is 38.2% or 41.4% depending on the RUWE threshold. The actual value should be higher since certain systems such as short-period binaries with low q remain undetected astrometrically and photometrically. All triple and higher-order systems were counted only once, meaning no more than $\sim 60\%$ of Pleiades stars with $m > 0.5 M_{\odot}$ are single. For the

field $0.75 < M < 1.25 M_{\odot}$ sample, M. Moe & R. Di Stefano (2017) obtained that $63 \pm 4\%$ of stars have no companions with $q > 0.1$. However, this comparison is crude, since $q < 0.1$ systems may show RUWE excess in the Pleiades (Figure 3) and thus be counted as binaries.

8. CONCLUSIONS

The major conclusions are drawn as follows:

- Binaries with near-twin components ($q \sim 1$) are more likely to get astrometric solution with small deviations and low RUWE relative to systems with intermediate mass ratios of $q \sim 0.5$. The latter are disfavored during cluster member selection. The induced bias varies between clusters and disturbs comparison of multiplicity statistics (Section 4.4).
- Photometrically estimated mass ratio is underestimated relative to spectroscopic (Section 6.3).
- Parallaxes inferred from non-single star solutions (Section 5) show worse convergence around the cluster mean compared to the single star solutions in Gaia DR3 for the same sources (Figure 4).
- An area of enlarged extinction (Figure 7) is traced by observed polarization; it compromises the photometric study of multiplicity (Sections 6.4 – 6.6).
- The inferred binary fraction for $q > 0.6$ systems is $f = 16.4\%^{+2.6}_{-0.6}$, which is compatible with the field population estimate (Section 7.2), but larger than most literature values for the Pleiades (Table 3).
- The binary fraction presumably does not increase with stellar mass in the $0.5 - 1.2 M_{\odot}$ range (Section 7.4). The mass ratio has a bimodal distribution with a minimum around $q \sim 0.7$ (Figure 11).

Table 4. Pleiades sample source list

Column	Units	Description
Gaia		Gaia DR3 designation
Gmag	mag	Gaia DR3 G magnitude
RUWE		Gaia DR3 parameter RUWE
ϖ	mas	Gaia DR3 reported parallax
q		Adopted mass ratio of the binary system
q_{\min}		Lower bound of q
q_{\max}		Upper bound of q
Type		Type of binarity: G: Resolved in Gaia DR3, I: Resolved with speckle observations (D. Chulkov et al. 2025), S: SB2 (Table 1), p: photometric, RUWE < 1.2, P: photometric, RUWE \geq 1.2 (Section 6)
q^{ϖ}		Photometrically fitted q (Section 6.2); $1/\varpi$ distance is assumed
m_1^{ϖ}	M_{\odot}	Best-fit mass of the primary star; $1/\varpi$ distance is assumed
χ^{ϖ}	mag	Photometric residual (Equation 5); $1/\varpi$ distance is assumed
q^C		Photometrically fitted q (Section 6.2); 135.6 pc distance is assumed
m_1^C	M_{\odot}	Best-fit mass of the primary star; 135.6 pc distance is assumed
χ^C	mag	Photometric residual (Equation 5); 135.6 pc distance is assumed
Trun		Primary mass truncation flag, $m_1 < 0.5M_{\odot}$ (Section 7.1) [1,0]
Ext		High extinction area flag (Section 6.6) [1,0]
Sec		Secondary source flag (Section 7.1) [1,0]
Mult		Triple or higher-order system flag (Section 7.1) [1,0]
nss		Gaia DR3 non-single star solution flag (Table 2) [1,0]
SB		Spectroscopic binarity type, based on Table 1 and G. Torres et al. (2021) [3,2,1,0]
Wide		Resolved companion flag (D. Chulkov et al. 2025) [1,0]
BF		Subsample adopted for binary fraction calculation (Section 7.1) [1,0]

NOTE—The input list is based on table 2 of D. Chulkov (2024). Stellar binarity is probed with several indicators; sources with an upper bound on adopted mass ratio $q_{\max} > 0.5$ are covered. Photometric mass ratios (Section 6) are considered unreliable and are omitted for bright stars ($G < 5$ mag) and resolved systems (Section 6.2.1). Two options are explored for the adopted distance, either based on reported parallax in Gaia DR3 or on the cluster mean value (Section 6.2). The inferred values of q^{ϖ} or q^C below 0.4 are set to zero as these sources are photometrically indistinguishable from single stars. Estimates of photometric mass ratio for the high extinction area are deemed unreliable; these sources are exempted from the binary fraction calculation (Section 6.6). (This entire table is available under the following link: https://github.com/chulkovd/Pleiades_revisited.)

ACKNOWLEDGMENTS

This work was largely inspired by the collaboration with Boris Safonov and Ivan Strakhov over the speckle interferometric survey of Pleiades at the SAI MSU observatory. The author is grateful to Alexey Sytov and Gabriel Perren for the discussion on CMD analysis and Zephyr Penoyre for insights on forward RUWE modeling. The author thanks the referee for a fast and smooth review.

Software: Aladin Lite (T. Boch & P. Fernique 2014; M. Baumann et al. 2022), Astrophysics Data System², astropy (Astropy Collaboration et al. 2013, 2018, 2022), CDS Cross-Match Service (T. Boch et al. 2012; F.-X. Pineau et al. 2020), GaiaUnlimited (A. Castro-Ginard et al. 2024), hips2fits³, ipyaladin (T. Boch & J. Desroziers 2020), SIMBAD (M. Wenger et al. 2000), TOPCAT (M. B. Taylor 2005), VizieR (F. Ochsenbein et al. 2000)

REFERENCES

² <https://ui.adsabs.harvard.edu/>

³ <https://alasky.cds.unistra.fr/hips-image-services/hips2fits>

- Adams, J. D., Stauffer, J. R., Monet, D. G., Skrutskie, M. F., & Beichman, C. A. 2001, *AJ*, 121, 2053, doi: [10.1086/319965](https://doi.org/10.1086/319965)
- Alexander, J. S., & Albrow, M. D. 2025, *MNRAS*, 536, 471, doi: [10.1093/mnras/stae2636](https://doi.org/10.1093/mnras/stae2636)
- Andersson, B. G., Lazarian, A., & Vaillancourt, J. E. 2015, *ARA&A*, 53, 501, doi: [10.1146/annurev-astro-082214-122414](https://doi.org/10.1146/annurev-astro-082214-122414)
- Astropy Collaboration, Robitaille, T. P., Tollerud, E. J., et al. 2013, *A&A*, 558, A33, doi: [10.1051/0004-6361/201322068](https://doi.org/10.1051/0004-6361/201322068)
- Astropy Collaboration, Price-Whelan, A. M., Sipőcz, B. M., et al. 2018, *AJ*, 156, 123, doi: [10.3847/1538-3881/aabc4f](https://doi.org/10.3847/1538-3881/aabc4f)
- Astropy Collaboration, Price-Whelan, A. M., Lim, P. L., et al. 2022, *ApJ*, 935, 167, doi: [10.3847/1538-4357/ac7c74](https://doi.org/10.3847/1538-4357/ac7c74)
- Baumann, M., Boch, T., Pineau, F.-X., et al. 2022, in *Astronomical Society of the Pacific Conference Series*, Vol. 532, *Astronomical Data Analysis Software and Systems XXX*, ed. J. E. Ruiz, F. Pierfederici, & P. Teuben, 7
- Belokurov, V., Penoyre, Z., Oh, S., et al. 2020, *MNRAS*, 496, 1922, doi: [10.1093/mnras/staa1522](https://doi.org/10.1093/mnras/staa1522)
- Bettis, C. 1975, *PASP*, 87, 707, doi: [10.1086/129832](https://doi.org/10.1086/129832)
- Boch, T., & Desrozier, J. 2020, in *Astronomical Society of the Pacific Conference Series*, Vol. 522, *Astronomical Data Analysis Software and Systems XXVII*, ed. P. Ballester, J. Ibsen, M. Solar, & K. Shortridge, 117
- Boch, T., & Fernique, P. 2014, in *Astronomical Society of the Pacific Conference Series*, Vol. 485, *Astronomical Data Analysis Software and Systems XXIII*, ed. N. Manset & P. Forshay, 277
- Boch, T., Pineau, F., & Derriere, S. 2012, in *Astronomical Society of the Pacific Conference Series*, Vol. 461, *Astronomical Data Analysis Software and Systems XXI*, ed. P. Ballester, D. Egret, & N. P. F. Lorente, 291
- Bouvier, J., Rigaut, F., & Nadeau, D. 1997, *A&A*, 323, 139
- Breger, M. 1986, *ApJ*, 309, 311, doi: [10.1086/164602](https://doi.org/10.1086/164602)
- Bressan, A., Marigo, P., Girardi, L., et al. 2012, *MNRAS*, 427, 127, doi: [10.1111/j.1365-2966.2012.21948.x](https://doi.org/10.1111/j.1365-2966.2012.21948.x)
- Cantat-Gaudin, T., & Casamiquela, L. 2024, *NewAR*, 99, 101696, doi: [10.1016/j.newar.2024.101696](https://doi.org/10.1016/j.newar.2024.101696)
- Cardelli, J. A., Clayton, G. C., & Mathis, J. S. 1989, *ApJ*, 345, 245, doi: [10.1086/167900](https://doi.org/10.1086/167900)
- Castro-Ginard, A., Penoyre, Z., Casey, A. R., et al. 2024, *A&A*, 688, A1, doi: [10.1051/0004-6361/202450172](https://doi.org/10.1051/0004-6361/202450172)
- Childs, A. C., & Geller, A. M. 2025, *ApJ*, 989, 104, doi: [10.3847/1538-4357/ade9bc](https://doi.org/10.3847/1538-4357/ade9bc)
- Childs, A. C., Geller, A. M., von Hippel, T., Motherway, E., & Zwicker, C. 2024, *ApJ*, 962, 41, doi: [10.3847/1538-4357/ad18c0](https://doi.org/10.3847/1538-4357/ad18c0)
- Choi, J., Dotter, A., Conroy, C., et al. 2016, *ApJ*, 823, 102, doi: [10.3847/0004-637X/823/2/102](https://doi.org/10.3847/0004-637X/823/2/102)
- Chulkov, D. 2024, *AJ*, 168, 156, doi: [10.3847/1538-3881/ad7025](https://doi.org/10.3847/1538-3881/ad7025)
- Chulkov, D., Strakhov, I., & Safonov, B. 2025, *AJ*, 169, 145, doi: [10.3847/1538-3881/ada564](https://doi.org/10.3847/1538-3881/ada564)
- Cifuentes, C., Caballero, J. A., González-Payo, J., et al. 2025, *A&A*, 693, A228, doi: [10.1051/0004-6361/202452527](https://doi.org/10.1051/0004-6361/202452527)
- Cordini, G., Milone, A. P., Marino, A. F., et al. 2023, *A&A*, 672, A29, doi: [10.1051/0004-6361/202245457](https://doi.org/10.1051/0004-6361/202245457)
- Cotton, D. V., Bailey, J., Kedziora-Chudczer, L., et al. 2024, *MNRAS*, 535, 1586, doi: [10.1093/mnras/stae2418](https://doi.org/10.1093/mnras/stae2418)
- Cournoyer-Cloutier, C., Sills, A., Harris, W. E., et al. 2024, *ApJ*, 977, 203, doi: [10.3847/1538-4357/ad90b3](https://doi.org/10.3847/1538-4357/ad90b3)
- David, T. J., & Hillenbrand, L. A. 2015, *ApJ*, 804, 146, doi: [10.1088/0004-637X/804/2/146](https://doi.org/10.1088/0004-637X/804/2/146)
- Donada, J., Anders, F., Jordi, C., et al. 2023, *A&A*, 675, A89, doi: [10.1051/0004-6361/202245219](https://doi.org/10.1051/0004-6361/202245219)
- Duchêne, G., & Kraus, A. 2013, *ARA&A*, 51, 269, doi: [10.1146/annurev-astro-081710-102602](https://doi.org/10.1146/annurev-astro-081710-102602)
- El-Badry, K. 2024, *NewAR*, 98, 101694, doi: [10.1016/j.newar.2024.101694](https://doi.org/10.1016/j.newar.2024.101694)
- El-Badry, K., Lam, C., Holl, B., et al. 2024, *The Open Journal of Astrophysics*, 7, 100, doi: [10.33232/001c.125461](https://doi.org/10.33232/001c.125461)
- El-Badry, K., Rix, H.-W., Ting, Y.-S., et al. 2018, *MNRAS*, 473, 5043, doi: [10.1093/mnras/stx2758](https://doi.org/10.1093/mnras/stx2758)
- Fabrizius, C., Luri, X., Arenou, F., et al. 2021, *A&A*, 649, A5, doi: [10.1051/0004-6361/202039834](https://doi.org/10.1051/0004-6361/202039834)
- Fitzpatrick, E. L., & Massa, D. 2007, *ApJ*, 663, 320, doi: [10.1086/518158](https://doi.org/10.1086/518158)
- Frasca, A., Zhang, J. Y., Alonso-Santiago, J., et al. 2025, *A&A*, 698, A7, doi: [10.1051/0004-6361/202553673](https://doi.org/10.1051/0004-6361/202553673)
- Gaia Collaboration, Prusti, T., de Bruijne, J. H. J., et al. 2016, *A&A*, 595, A1, doi: [10.1051/0004-6361/201629272](https://doi.org/10.1051/0004-6361/201629272)
- Gaia Collaboration, Brown, A. G. A., Vallenari, A., et al. 2021, *A&A*, 649, A1, doi: [10.1051/0004-6361/202039657](https://doi.org/10.1051/0004-6361/202039657)
- Gaia Collaboration, Vallenari, A., Brown, A. G. A., et al. 2023a, *A&A*, 674, A1, doi: [10.1051/0004-6361/202243940](https://doi.org/10.1051/0004-6361/202243940)
- Gaia Collaboration, Arenou, F., Babusiaux, C., et al. 2023b, *A&A*, 674, A34, doi: [10.1051/0004-6361/202243782](https://doi.org/10.1051/0004-6361/202243782)
- Gosset, E., Damerdj, Y., Morel, T., et al. 2025, *A&A*, 693, A124, doi: [10.1051/0004-6361/202450600](https://doi.org/10.1051/0004-6361/202450600)
- Grondin, S. M., Drout, M. R., Nordhaus, J., et al. 2024, *ApJ*, 976, 102, doi: [10.3847/1538-4357/ad7500](https://doi.org/10.3847/1538-4357/ad7500)
- Halbwachs, J.-L., Pourbaix, D., Arenou, F., et al. 2023, *A&A*, 674, A9, doi: [10.1051/0004-6361/202243969](https://doi.org/10.1051/0004-6361/202243969)

- Heyl, J., Caiazzo, I., & Richer, H. B. 2022, *ApJ*, 926, 132, doi: [10.3847/1538-4357/ac45fc](https://doi.org/10.3847/1538-4357/ac45fc)
- Holl, B., Fabricius, C., Portell, J., et al. 2023, *A&A*, 674, A25, doi: [10.1051/0004-6361/202245353](https://doi.org/10.1051/0004-6361/202245353)
- Hsu, J. C., & Breger, M. 1982, *ApJ*, 262, 732, doi: [10.1086/160467](https://doi.org/10.1086/160467)
- Jadhav, V. V., Roy, K., Joshi, N., & Subramaniam, A. 2021, *AJ*, 162, 264, doi: [10.3847/1538-3881/ac2571](https://doi.org/10.3847/1538-3881/ac2571)
- Jiang, Y., Zhong, J., Qin, S., et al. 2024, *ApJ*, 971, 71, doi: [10.3847/1538-4357/ad5344](https://doi.org/10.3847/1538-4357/ad5344)
- Jing, Y., Mao, T.-X., Wang, J., Liu, C., & Chen, X. 2025, *ApJS*, 277, 15, doi: [10.3847/1538-4365/ada895](https://doi.org/10.3847/1538-4365/ada895)
- Klement, R., Rivinius, T., Gies, D. R., et al. 2024, *ApJ*, 962, 70, doi: [10.3847/1538-4357/ad13ec](https://doi.org/10.3847/1538-4357/ad13ec)
- Kos, J. 2024, *A&A*, 691, A28, doi: [10.1051/0004-6361/202449828](https://doi.org/10.1051/0004-6361/202449828)
- Kounkel, M., Covey, K. R., Stassun, K. G., et al. 2021, *AJ*, 162, 184, doi: [10.3847/1538-3881/ac1798](https://doi.org/10.3847/1538-3881/ac1798)
- Li, S.-s., Li, C.-q., Li, C.-h., et al. 2025, *ApJS*, 276, 11, doi: [10.3847/1538-4365/ad9010](https://doi.org/10.3847/1538-4365/ad9010)
- Lindgren, L., Klioner, S. A., Hernández, J., et al. 2021, *A&A*, 649, A2, doi: [10.1051/0004-6361/202039709](https://doi.org/10.1051/0004-6361/202039709)
- Liu, R., Shao, Z., & Li, L. 2025, *AJ*, 169, 116, doi: [10.3847/1538-3881/ada380](https://doi.org/10.3847/1538-3881/ada380)
- Long, L., Bi, S., Zhang, J., et al. 2023, *ApJS*, 268, 30, doi: [10.3847/1538-4365/ace5af](https://doi.org/10.3847/1538-4365/ace5af)
- Longhin, A. 2025, arXiv e-prints, arXiv:2503.12543, doi: [10.48550/arXiv.2503.12543](https://doi.org/10.48550/arXiv.2503.12543)
- Maíz Apellániz, J. 2024, arXiv e-prints, arXiv:2401.01116, doi: [10.48550/arXiv.2401.01116](https://doi.org/10.48550/arXiv.2401.01116)
- Makarov, V. V. 2025, *ApJL*, 981, L23, doi: [10.3847/2041-8213/adb840](https://doi.org/10.3847/2041-8213/adb840)
- Malofeeva, A. A., Mikhnevich, V. O., Carraro, G., & Seleznev, A. F. 2023, *AJ*, 165, 45, doi: [10.3847/1538-3881/aca666](https://doi.org/10.3847/1538-3881/aca666)
- Mardling, R. A., & Aarseth, S. J. 2001, *MNRAS*, 321, 398, doi: [10.1046/j.1365-8711.2001.03974.x](https://doi.org/10.1046/j.1365-8711.2001.03974.x)
- Mészáros, S., Jofré, P., Johnson, J. A., et al. 2025, *AJ*, 170, 96, doi: [10.3847/1538-3881/ade4b9](https://doi.org/10.3847/1538-3881/ade4b9)
- Moe, M., & Di Stefano, R. 2017, *ApJS*, 230, 15, doi: [10.3847/1538-4365/aa6fb6](https://doi.org/10.3847/1538-4365/aa6fb6)
- Nagarajan, P., & El-Badry, K. 2024, *PASP*, 136, 094203, doi: [10.1088/1538-3873/ad7981](https://doi.org/10.1088/1538-3873/ad7981)
- Nemravová, J., Harmanec, P., Kubát, J., et al. 2010, *A&A*, 516, A80, doi: [10.1051/0004-6361/200913885](https://doi.org/10.1051/0004-6361/200913885)
- Nguyen, C. T., Costa, G., Girardi, L., et al. 2022, *A&A*, 665, A126, doi: [10.1051/0004-6361/202244166](https://doi.org/10.1051/0004-6361/202244166)
- Niu, H., Wang, J., & Fu, J. 2020, *ApJ*, 903, 93, doi: [10.3847/1538-4357/abb8d6](https://doi.org/10.3847/1538-4357/abb8d6)
- Ochsenbein, F., Bauer, P., & Marcout, J. 2000, *A&AS*, 143, 23, doi: [10.1051/aas:2000169](https://doi.org/10.1051/aas:2000169)
- O'Donnell, J. E. 1994, *ApJ*, 422, 158, doi: [10.1086/173713](https://doi.org/10.1086/173713)
- Offner, S. S. R., Moe, M., Kratter, K. M., et al. 2023, in *Astronomical Society of the Pacific Conference Series*, Vol. 534, *Protostars and Planets VII*, ed. S. Inutsuka, Y. Aikawa, T. Muto, K. Tomida, & M. Tamura, 275, doi: [10.48550/arXiv.2203.10066](https://doi.org/10.48550/arXiv.2203.10066)
- Pang, X., Wang, Y., Tang, S.-Y., et al. 2023, *AJ*, 166, 110, doi: [10.3847/1538-3881/ace76c](https://doi.org/10.3847/1538-3881/ace76c)
- Penoyre, Z., Belokurov, V., & Evans, N. W. 2022, *MNRAS*, 513, 2437, doi: [10.1093/mnras/stac959](https://doi.org/10.1093/mnras/stac959)
- Penoyre, Z., Belokurov, V., Wyn Evans, N., Everall, A., & Koposov, S. E. 2020, *MNRAS*, 495, 321, doi: [10.1093/mnras/staa1148](https://doi.org/10.1093/mnras/staa1148)
- Perryman, M. 2025, arXiv e-prints, arXiv:2509.10883, doi: [10.48550/arXiv.2509.10883](https://doi.org/10.48550/arXiv.2509.10883)
- Pineau, F.-X., Boch, T., Derrière, S., & Schaaff, A. 2020, in *Astronomical Society of the Pacific Conference Series*, Vol. 522, *Astronomical Data Analysis Software and Systems XXVII*, ed. P. Ballester, J. Ibsen, M. Solar, & K. Shortridge, 125
- Pinfield, D. J., Dobbie, P. D., Jameson, R. F., et al. 2003, *MNRAS*, 342, 1241, doi: [10.1046/j.1365-8711.2003.06630.x](https://doi.org/10.1046/j.1365-8711.2003.06630.x)
- Raghavan, D., McAlister, H. A., Henry, T. J., et al. 2010, *ApJS*, 190, 1, doi: [10.1088/0067-0049/190/1/1](https://doi.org/10.1088/0067-0049/190/1/1)
- Reggiani, M., & Meyer, M. R. 2013, *A&A*, 553, A124, doi: [10.1051/0004-6361/201321631](https://doi.org/10.1051/0004-6361/201321631)
- Riello, M., De Angeli, F., Evans, D. W., et al. 2021, *A&A*, 649, A3, doi: [10.1051/0004-6361/202039587](https://doi.org/10.1051/0004-6361/202039587)
- Risbud, D., Jadhav, V. V., & Kroupa, P. 2025, *A&A*, 694, A258, doi: [10.1051/0004-6361/202453302](https://doi.org/10.1051/0004-6361/202453302)
- Roeser, S., Demleitner, M., & Schilbach, E. 2010, *AJ*, 139, 2440, doi: [10.1088/0004-6256/139/6/2440](https://doi.org/10.1088/0004-6256/139/6/2440)
- Sairam, L., Baycroft, T. A., Boisse, I., et al. 2024, *MNRAS*, 534, 3999, doi: [10.1093/mnras/stae2317](https://doi.org/10.1093/mnras/stae2317)
- Sana, H., & Vrancken, J. 2025, arXiv e-prints, arXiv:2504.00548, doi: [10.48550/arXiv.2504.00548](https://doi.org/10.48550/arXiv.2504.00548)
- SDSS Collaboration, Adamane Pallathadka, G., Aghakhanloo, M., et al. 2025, arXiv e-prints, arXiv:2507.07093, doi: [10.48550/arXiv.2507.07093](https://doi.org/10.48550/arXiv.2507.07093)
- Serkowski, K., Mathewson, D. S., & Ford, V. L. 1975, *ApJ*, 196, 261, doi: [10.1086/153410](https://doi.org/10.1086/153410)
- Skrutskie, M. F., Cutri, R. M., Stiening, R., et al. 2006, *AJ*, 131, 1163, doi: [10.1086/498708](https://doi.org/10.1086/498708)
- Southworth, J. 2020, in *Stars and their Variability Observed from Space*, ed. C. Neiner, W. W. Weiss, D. Baade, R. E. Griffin, C. C. Lovekin, & A. F. J. Moffat, 329–334, doi: [10.48550/arXiv.1912.13400](https://doi.org/10.48550/arXiv.1912.13400)

- Stassun, K. G., & Torres, G. 2021, *ApJL*, 907, L33,
doi: [10.3847/2041-8213/abdaad](https://doi.org/10.3847/2041-8213/abdaad)
- Susemihl, N., & Meyer, M. R. 2022, *A&A*, 657, A48,
doi: [10.1051/0004-6361/202038582](https://doi.org/10.1051/0004-6361/202038582)
- Taylor, B. J. 2008, *AJ*, 136, 1388,
doi: [10.1088/0004-6256/136/3/1388](https://doi.org/10.1088/0004-6256/136/3/1388)
- Taylor, M. B. 2005, in *Astronomical Society of the Pacific Conference Series*, Vol. 347, *Astronomical Data Analysis Software and Systems XIV*, ed. P. Shopbell, M. Britton, & R. Ebert, 29
- Tokovinin, A. 2021, *Universe*, 7, 352,
doi: [10.3390/universe7090352](https://doi.org/10.3390/universe7090352)
- Torres, G. 2020, *ApJ*, 901, 91,
doi: [10.3847/1538-4357/abb136](https://doi.org/10.3847/1538-4357/abb136)
- Torres, G., Latham, D. W., & Quinn, S. N. 2021, *ApJ*, 921, 117, doi: [10.3847/1538-4357/ac1585](https://doi.org/10.3847/1538-4357/ac1585)
- Torres, G., Melis, C., Kraus, A. L., et al. 2020, *ApJ*, 898, 2,
doi: [10.3847/1538-4357/ab9c20](https://doi.org/10.3847/1538-4357/ab9c20)
- Torres, G., Tkachenko, A., Pavlovski, K., et al. 2025, *ApJ*, 990, 107, doi: [10.3847/1538-4357/adf224](https://doi.org/10.3847/1538-4357/adf224)
- Voshchinnikov, N. V. 2012, *JQSRT*, 113, 2334,
doi: [10.1016/j.jqsrt.2012.06.013](https://doi.org/10.1016/j.jqsrt.2012.06.013)
- Wallace, A. L. 2024, *MNRAS*, 527, 8718,
doi: [10.1093/mnras/stad3789](https://doi.org/10.1093/mnras/stad3789)
- Wang, F., Fang, M., Fu, X., et al. 2025, *ApJ*, 979, 92,
doi: [10.3847/1538-4357/ad960a](https://doi.org/10.3847/1538-4357/ad960a)
- Wenger, M., Ochsenbein, F., Egret, D., et al. 2000, *A&AS*, 143, 9, doi: [10.1051/aas:2000332](https://doi.org/10.1051/aas:2000332)
- Wilson, O. C. 1941, *ApJ*, 93, 29, doi: [10.1086/144239](https://doi.org/10.1086/144239)
- Wright, E. L., Eisenhardt, P. R. M., Mainzer, A. K., et al. 2010, *AJ*, 140, 1868, doi: [10.1088/0004-6256/140/6/1868](https://doi.org/10.1088/0004-6256/140/6/1868)